Analytical Investigation of the Dynamics of Tethered Constellations in Earth Orbit (Phase II)

Contract NAS8-36606

Quarterly Report #3

For the period 22 September 1985 through 21 December 1985

Principal Investigator

Dr. Enrico Lorenzini

February 1986

Prepared for
National Aeronautics and Space Administration
Marshall Space Flight Center, Alabama 35812

Smithsonian Institution
Astrophysical Observatory
Cambridge, Massachusetts 02138

The Smithsonian Astrophysical Observatory
is a member of the
Harvard-Smithsonian Center for Astrophysics

CONTENTS

Analytical Investigation of the Dynamics of Tethered Constellations in Earth Orbit (Phase II)

Contract NAS8-36606

Quarterly Report #3

For the period 22 September 1985 through 21 December 1985

Principal Investigator
Dr. Enrico Lorenzini

Co-Investigators
Mr. David A. Arnold
Dr. Mario D. Grossi
Dr. Gordon E. Gullahorn

February 1986

Prepared for
National Aeronautics and Space Administration
Marshall Space Flight Center, Alabama 35812

Smithsonian Institution
Astrophysical Observatory
Cambridge, Massachusetts 02138

Abstract

This quarterly report deals with the development of a two-dimensional analytical model that describes the dynamics of an n-mass vertical tethered system. Two different approaches are described: in the first one the control quantities are the independent variables while in the second one the Cartesian coordinates of each mass expressed in the orbiting reference frame are the independent variables. The latter model has been used in the 3-mass version to simulate the dynamics of the tethered system in applications involving the displacement of the middle mass along the tether. In particular the issues related to reproducing predetermined acceleration profiles and "g-tuning" are reported.

Figure Captions

Figure 2.1.1 Geometry and generalized coordinates for the n-mass tethered system.

Figure 2.3.1 Geometry and Cartesian coordinates for the n-mass tethered system.

Figure 2.3.2 Schematic of the tension forces acting on a single mass of an n-mass tethered system.

Figure 2.3.3 Geometrical relations between generalized coordinates and Cartesian coordinates.

Figure 2.5.1 a-l Dynamic response of the 3-mass tethered system for a sinusoidal motion of the middle mass with a peak-to-peak amplitude of 2000 m and an angular frequency of 10^{-3} rad/sec.

Figure 2.5.2 a-l Same as in Figure 2.5.1 with a peak-to-peak amplitude of the motion of the middle mass equal to 8000 m.

Figure 2.6.1 a-m Dynamic response of the 3-mass tethered system during a transfer maneuver of the middle mass designed for achieving a predetermined, steady state g-level ("g-tuning"). The control law is a half cycle sinusoid with a peak-to-peak amplitude of 2000 m.

Figure 2.6.2 a-m Same as in Figure 2.6.1 with a control law of different type. A modified hyperbolic tangent is used to perform the transfer maneuver instead of the half cycle sinusoid.

1.0 INTRODUCTION

This is the third Quarterly Report submitted by SAO under contract NAS8-36606, "Analytical Investigation of the Dynamics of Tethered Constellations in Earth Orbit (Phase II)," Dr. Enrico Lorenzini, PI. It covers the period from 22 September 1985 through 21 December 1985.

2.0 TECHNICAL ACTIVITY DURING REPORTING PERIOD AND PROGRAM STATUS

2.1 Two-Dimensional Equations Of Motion For The N-Mass System

The Lagrangian formulation has been used to derive the two-dimensional equations of motion for an n-mass tethered system. The equations of motion are expressed in the orbiting reference frame formed by the local vertical (z) and the local horizon (x) centered at the system C.M. The Lagrangian coordinates, shown in Figure 2.1.1, are the tether lengths (ℓ_i), the deflections (ϵ_i) of each mass from the line connecting the first mass to the last mass and the angle (θ) between that line and the local vertical. The assumptions are like those used for the 3-mass system, namely: point masses, circular orbit of the C.M., second order gravity potential expansion, elastic tethers. Following a procedure similar to the one in Quarterly Report #1 and referring to Figure 2.1.1, the kinetic energy of the system is given by:

$$T = \frac{1}{2}\sum_{i}^{n} m_i \left| \vec{v}_{Ii} \right|^2 \qquad (2.1.1)$$

In equation (2.1.1) the velocity of the i^{th}-mass is given by:

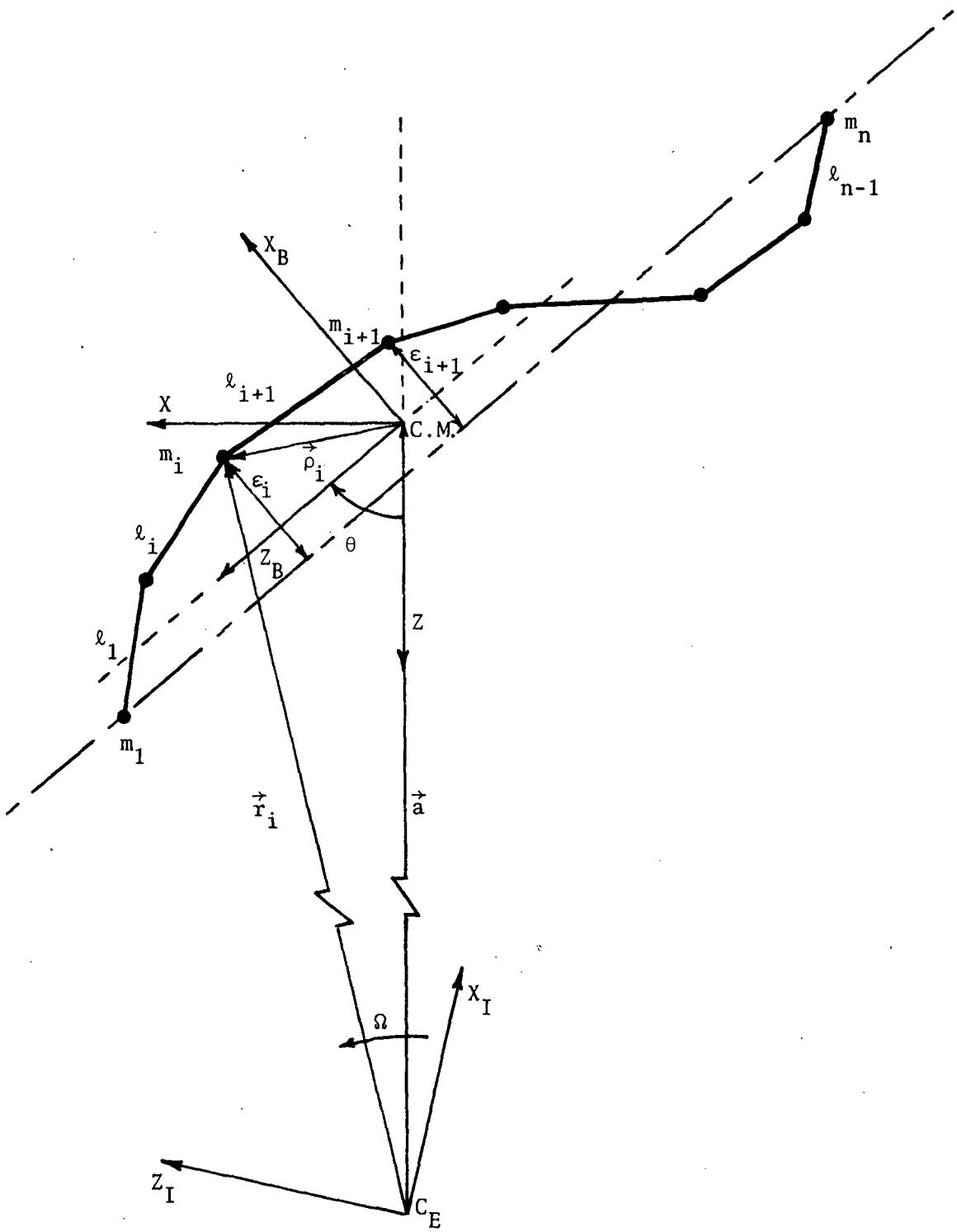
m_n
ℓ_{n-1}
X_B
m_{i+1}
ε_{i+1}
ℓ_{i+1}
X
C.M.
m_i
$\vec{\rho}_i$
ε_i
ℓ_i
Z_B
θ
Z
ℓ_1
m_1
$\vec{r}_i$
$\vec{a}$
X_I
Ω
Z_I
C_E

Figure 2.1.1

$$\vec{v}_{Ii} = \vec{v}_i + (\vec{\Omega} \times \vec{r}_i) \tag{2.1.2}$$

and since we have:

$$\vec{v}_i = \vec{v}_{Bi} + (\dot{\vec{\theta}} \times \vec{\rho}_{Bi}) \tag{2.1.3}$$

$$\vec{r}_i = \vec{a} + \vec{\rho}_i \tag{2.1.4}$$

we can write equation (2.1.2) as follows:

$$\vec{v}_{Ii} = \vec{v}_{Bi} + (\vec{\Omega} \times \vec{a}) + (\dot{\vec{\theta}} + \vec{\Omega}) \times \vec{\rho}_{Bi} \tag{2.1.5}$$

so that:

$$|\vec{v}_{Ii}|^2 = [\dot{x}_{Bi} + \Omega a \cos\theta + (\dot{\theta} - \Omega) z_{Bi}]^2 + [\dot{z}_{Bi} + \Omega a \sin\theta - (\dot{\theta} - \Omega) x_{Bi}]^2 \tag{2.1.6}$$

Since the body reference frame is centered at the system C.M. we have:

$$\sum_1^n m_i \, x_{Bi} = \sum_1^n m_i \, z_{Bi} = 0 \tag{2.1.7}$$

Moreover, since the C.M. remains, through time, at the center of the orbiting reference frame we also have:

$$\sum_1^n m_i \, \dot{x}_{Bi} = \sum_1^n m_i \, \dot{z}_{Bi} = 0 \tag{2.1.8}$$

By manipulating equation (2.1.6) we finally get:

$$T = \frac{1}{2}\sum_{1}^{n} m_i \left\{\dot{x}_{Bi}^2 + \dot{z}_{Bi}^2 + (\dot{\theta} - \Omega)^2 (x_{Bi}^2 + z_{Bi}^2) + 2(\dot{\theta} - \Omega)(\dot{x}_{Bi} z_{Bi} - x_{Bi}\dot{z}_{Bi})\right\} + \frac{1}{2} m_{tot}\Omega^2 a^2 \qquad (2.1.9)$$

where the last term is the kinetic energy of the system concentrated at the C.M.

The potential energy of the system is given by:

$$V = -\mu \sum_{1}^{n} \frac{m_i}{|r_i|} \qquad (2.1.10)$$

where:

$$|r_i| = \left[x_i^2 + (a - z_i)^2\right]^{1/2} \qquad (2.1.11)$$

We can therefore write the potential energy as:

$$V = -\mu \sum_{1}^{n} m_i \left[1 + \frac{z_i}{a} - \frac{x_{Bi}^2 + z_{Bi}^2}{2a^2} + \frac{3}{2}\frac{z_i^2}{a^2}\right] \qquad (2.1.12)$$

where:

$$x_{Bi}^2 + z_{Bi}^2 = x_i^2 + z_i^2 \qquad (2.1.13)$$

Since:

$$\mu = \Omega^2 a^3$$

$$z_i = z_{Bi}\cos\theta - x_{Bi}\sin\theta \qquad (2.1.14)$$

after algebraic manipulations and because of equations (2.1.7) we finally get:

$$V = -\frac{1}{2}\sum_{1}^{n} m_i\Big\{\Omega^2(3\cos^2\theta - 1)z_{Bi}^2 + \Omega^2(3\sin^2\theta - 1)x_{Bi}^2 - 6\,\Omega^2\sin\theta\cos\theta\,x_{Bi}z_{Bi}\Big\} - m_{tot}\Omega^2a^2 \qquad (2.1.15)$$

In equation (2.1.15) the last term is the potential energy of the system when the total mass is concentrated at the C.M.; its value is constant for a circular orbit.

Assuming that $\epsilon_i \ll \ell_i$ and defining $R_i = m_i/m_{tot}$ we can write:

$$\begin{aligned} z_{B1} &= -z_{BCM1} \\ z_{B2} &= \ell_1 - z_{BCM1} \\ &\vdots \\ z_{Bi} &= \sum_{j=1}^{i}\ell_j - z_{BCM1} \\ &\vdots \\ z_{Bn} &= \sum_{j=1}^{n-1}\ell_j - z_{BCM1} \end{aligned} \qquad (2.1.16)$$

and:

$$\begin{aligned} x_{B1} &= -x_{BCM1} \\ x_{B2} &= \epsilon_1 - x_{BCM1} \\ &\vdots \\ x_{Bi} &= \epsilon_i - x_{BCM1} \\ &\vdots \\ x_{Bn} &= -x_{BCM1} \end{aligned} \qquad (2.1.17)$$

where z_{BCM1} and x_{BCM1} are the coordinates, in a body reference frame with the origin at m_1, of the system C.M. They can be expressed as follows:

$$z_{BCM1} = R_{(2,\ldots,n)}\ \ell_1 + \ldots. + R_n \ell_{n-1}$$

$$x_{BCM1} = \sum_{j=1}^{n-2} R_{j+1}\ \epsilon_j \qquad (2.1.18)$$

where:

$$R_{(i,\ldots,n)} = \sum_{j=i}^{n} R_j \qquad (2.1.19)$$

Equations (2.1.16) and (2.1.17) relate the coordinates of the masses in body axis to the Lagrangian coordinates.

The Lagrangian function (L) is readily obtained by subtracting the potential energy from the kinetic energy so that the equations of motion are given by:

$$\frac{d}{dt}\left(\frac{\partial L}{\partial \dot{\ell}_i}\right) - \frac{\partial L}{\partial \ell_i} = Q_{\ell_i} \qquad i = 1,\ldots,n$$

$$\frac{d}{dt}\left(\frac{\partial L}{\partial \dot{\epsilon}_i}\right) - \frac{\partial L}{\partial \epsilon_i} = Q_{\epsilon_i} \qquad i = 1,\ldots,n-1 \qquad (2.1.20)$$

$$\frac{d}{dt}\left(\frac{\partial L}{\partial \dot{\theta}}\right) - \frac{\partial L}{\partial \theta} = Q_\theta$$

After many algebraic manipulations the final structure of the equations of motion is as follows:

$$\mathbf{A}[\ddot{\boldsymbol{\ell}} + b\boldsymbol{\ell}] + 2(\dot{\theta} - \Omega)\ \mathbf{B}\ \dot{\boldsymbol{\epsilon}} + (\ddot{\theta} - d)\ \mathbf{C}\ \boldsymbol{\epsilon} = Q_{\ell_i}/m_{tot}$$

$$\mathbf{D}[\ddot{\boldsymbol{\epsilon}} + g\boldsymbol{\epsilon}] + 2(\dot{\theta} - \Omega)\ \mathbf{E}\ \dot{\boldsymbol{\ell}} + (\ddot{\theta} + d)\ \mathbf{F}\ \boldsymbol{\ell} = Q_{\epsilon_i}/m_{tot} \qquad (2.1.21)$$

$$\mathbf{G}[\ddot{\theta},\ 2(\dot{\theta} - \Omega),\ 3\Omega^2 \sin\theta\cos\theta,\ 3\Omega^2(\sin^2\theta - \cos^2\theta)]^T + \boldsymbol{\epsilon}\mathbf{H}\ddot{\boldsymbol{\ell}} + \boldsymbol{\ell}\mathbf{L}\ddot{\boldsymbol{\epsilon}} = Q_\theta/m_{tot}$$

In equations (2.1.21) $\boldsymbol{\ell}$, $\dot{\boldsymbol{\ell}}$, $\ddot{\boldsymbol{\ell}}$ are column vectors of dimension n-1 and $\boldsymbol{\epsilon}$, $\dot{\boldsymbol{\epsilon}}$, $\ddot{\boldsymbol{\epsilon}}$ are also column vectors of dimension n-1 with the last row equal to zero. The matrices **A**, **B**, **C**, **D**, **E**, **F**, **H**, **L** are non dimensional matrices and **G** is on the contrary dimensional, being a function of $\boldsymbol{\epsilon}$, $\dot{\boldsymbol{\epsilon}}$, $\boldsymbol{\ell}$, $\dot{\boldsymbol{\ell}}$. Their complex expressions are not reported in this quarterly report for the sake of brevity. The coefficients in equations (2.1.21) are given by:

$$\begin{aligned} b &= \Omega^2\ (1-3\cos^2\theta)\ -\ (\dot{\theta}-\Omega)^2 \\ d &= 3\Omega^2 \sin\theta\cos\theta \\ g &= \Omega^2(1-3\sin^2\theta)\ -\ (\dot{\theta}-\Omega)^2 \end{aligned} \qquad (2.1.22)$$

The equations of motion (2.1.21) together with (2.1.22) will be fully developed in the next section for the case n=3. Note that equations (2.1.22) are a set of 2(n-1) equations while in general the degrees of freedom of n masses in a two-dimensional space are 2n. In our case, however, the motion of the system C.M. is constrained so that the total degrees of freedom of the system are 2n-2.

2.2 Revised Two-Dimensional Equations Of Motion For The 3-Mass System

From the generalized case of the previous section we derive in this section the equations of motion for a 3-mass system. The tedious computation of the matrix components in equation (2.1.21) is not reported. The equations of motion finally result in:

$$R_1(1-R_1)\ [\ddot{\ell}_1 + b\ell_1] + R_1R_3\ [\ddot{\ell}_2 + b\ell_2] - 2(\dot{\theta}-\Omega)R_1R_2\dot{\epsilon} - (\ddot{\theta}-d)R_1R_2\epsilon = Q_{\ell_1}/m_{tot}$$

$$R_3(1-R_3)\ [\ddot{\ell}_2 + b\ell_2] + R_1R_3\ [\ddot{\ell}_1 + b\ell_1] + 2(\dot{\theta}-\Omega)R_2R_3\dot{\epsilon} + (\ddot{\theta}-d)R_2R_3\epsilon = Q_{\ell_2}/m_{tot}$$

$$R_2(1-R_2)\ [\ddot{\epsilon} + g\epsilon] - 2(\dot{\theta}-\Omega)R_2\dot{v} - (\ddot{\theta}+d)R_2v = Q_\epsilon/m_{tot} \qquad (2.1.23)$$

$$\begin{aligned}
&\ddot{\theta}\left\{R_1\ell_1[\ell_1+v]+R_3\ell_2[\ell_2-v]+R_2(1-R_2)\,\epsilon^2\right\}+\\
&+\ 2(\dot{\theta}-\Omega)\left\{R_1\ell_1[\dot{\ell}_1+\dot{v}]+R_3\ell_2[\dot{\ell}_2-\dot{v}]+R_2(1-R_2)\,\epsilon\dot{\epsilon}\right\}+\\
&+\ 3\Omega^2\sin\theta\cos\theta\left\{R_1\ell_1[\ell_1+v]+R_3\ell_2[\ell_2-v]-R_2(1-R_2)\,\epsilon^2\right\}+\\
&+\ 3\Omega^2(\sin^2\theta-\cos^2\theta)R_2v\epsilon-R_2\epsilon\left\{R_1\ddot{\ell}_1-R_3\ddot{\ell}_2\right\}-R_2\ddot{\epsilon}v = Q_\theta/m_{tot}
\end{aligned}$$

where b, d and g are given by equations (2.1.22) while v and $\dot{v}$ are given by:

$$\begin{aligned} v &= R_3\ell_2 - R_1\ell_1 \\ \dot{v} &= R_3\dot{\ell}_2 - R_1\dot{\ell}_1 \end{aligned} \qquad (2.1.24)$$

The generalized forces had already been derived in Quarterly Report #1; they are given by:

$$\begin{aligned} Q_{\ell_1} &= -T_1 \\ Q_{\ell_2} &= -T_2 \\ Q_\epsilon &= -\epsilon(T_1/\ell_1 + T_2/\ell_2) \\ Q_\theta &= 0 \end{aligned} \qquad (2.1.25)$$

A comparison of equations (2.1.23) with equations (2.1.15) of Quarterly Report #1, taking into account the different notation, shows that some inaccuracies were present in the latter equations. However those inaccuracies involved terms which multiplied v or $\dot{v}$. v and $\dot{v}$ represent the distance of m_2 from the system C.M. and its rate of change respectively. In all the simulations reported in Quarterly Reports #1 and #2 the values of v and $\dot{v}$ were zero or close to it so that the results shown in those reports are correct. As a confirmation of this we ran with the new model one of the case reported in Quarterly Report #2 obtaining the same results. When simulating the middle mass travelling along the tether the incorrect terms are, on the contrary, important and the use of the new model is therefore mandatory.

In equations (2.1.23) the independent variables are the controlled or the observed parameters. To associate control laws to the system equations is therefore a straight forward process. Equations (2.1.23), however, have the disadvantage of being non-normalized. In matrix form the equations (2.1.23) can be written:

$$\mathbf{A}\,\ddot{\mathbf{x}} = \mathbf{b} \qquad (2.1.26)$$

where $\ddot{\mathbf{x}} = [\ddot{\theta},\ \ddot{\epsilon},\ \ddot{\ell}_1,\ \ddot{\ell}_2]^T$, $\mathbf{A}$ is a symmetric 4x4 matrix and $\mathbf{b} = [b_1,\ b_2,\ b_3,\ b_4]^T$. The numerical integration of equations (2.1.26) implies the inversion of matrix $\mathbf{A}$. Even if it is not a problem for a 4x4 matrix, the inversion becomes more and more time consuming for bigger matrices (greater number of masses). For this reason a different model in Cartesian coordinates has been derived, as shown in the next section. For the sake of completeness the components of matrices $\mathbf{A}$ and $\mathbf{b}$ are given below:

$$
\begin{aligned}
a_{11} &= R_1\ell_1[\ell_1+v]+R_3\ell_2[\ell_2-v]+R_2(1-R_2)\epsilon^2 \\
a_{22} &= R_2(1-R_2) \\
a_{33} &= R_1(1-R_1) \\
a_{44} &= R_3(1-R_3) \\
a_{12} &= a_{21} = -R_2v \\
a_{13} &= a_{31} = -R_1R_2\epsilon \\
a_{14} &= a_{41} = R_2R_3\epsilon \\
a_{23} &= a_{32} = 0 \\
a_{24} &= a_{42} = 0 \\
a_{34} &= a_{43} = R_1R_3
\end{aligned}
\qquad (2.1.27)
$$

$$
\begin{aligned}
b_1 &= -2(\dot\theta-\Omega)\left\{R_1\ell_1[\dot\ell_1+\dot v]+R_3\ell_2[\dot\ell_2-\dot v]+R_2(1-R_2)\epsilon\dot\epsilon\right\}- \\
&\quad d\left\{R_1\ell_1[\ell_1+v]+R_3\ell_2[\ell_2-v]-R_2(1-R_2)\epsilon^2\right\}-3\Omega^2(\sin^2\theta-\cos^2\theta)R_1\epsilon v \\
b_2 &= Q_\epsilon/m_{tot} - R_2(1-R_2)g\,\epsilon + 2(\dot\theta-\Omega)R_2\dot v + dR_2v \\
b_3 &= Q_{\ell_1}/m_{tot} - b[R_1(1-R_1)\ell_1 + R_1R_3\ell_2] + 2(\dot\theta-\Omega)R_1R_2\dot\epsilon - dR_1R_2\epsilon \\
b_4 &= Q_{\ell_2}/m_{tot} - b[R_3(1-R_3)\ell_2+R_1R_3\ell_1] - 2(\dot\theta-\Omega)R_2R_3\dot\epsilon + dR_2R_3\epsilon
\end{aligned}
\qquad (2.1.28)
$$

Equations (2.1.27) and (2.1.28) are complemented by equations (2.1.25), (2.1.24) and (2.1.22).

2.3 Another Model For The N-Mass System. Cartesian Coordinate Equations Of Motion

The model derived in the previous section is very convenient from the control viewpoint since the variables of the system equations are the control parameters. However, because of the difficulty of inverting large matrices, this model's numerical integration is not efficient. In this section, we will therefore develop the equations of motion for a two-dimensional, n-mass tethered system in Cartesian coordinates relative to the orbiting reference frame. The equations in this form can be directly integrated without matrix inversion; on the other end the relations between the system variables and the controlled/observed variables are much more complex.

Referring to Figure 2.3.1 let us define the radius vector of the generic i^{th}-mass as follows:

$$\vec{r}_i = \vec{a} + \vec{\rho}_i \tag{2.3.1}$$

where:

$$\vec{\rho}_i = x_i \vec{I} + z_i \vec{k}$$

$$\vec{a} = -a\vec{k} \tag{2.3.2}$$

In the case of Ω = constant we can write the inertial acceleration of the i^{th}-mass as follows:

$$\ddot{\vec{r}}_{Ii} = \ddot{\vec{\rho}}_i + 2\vec{\Omega} \times \dot{\vec{\rho}}_i + \vec{\Omega} \times (\vec{\Omega} \times \vec{r}_i) \tag{2.3.3}$$

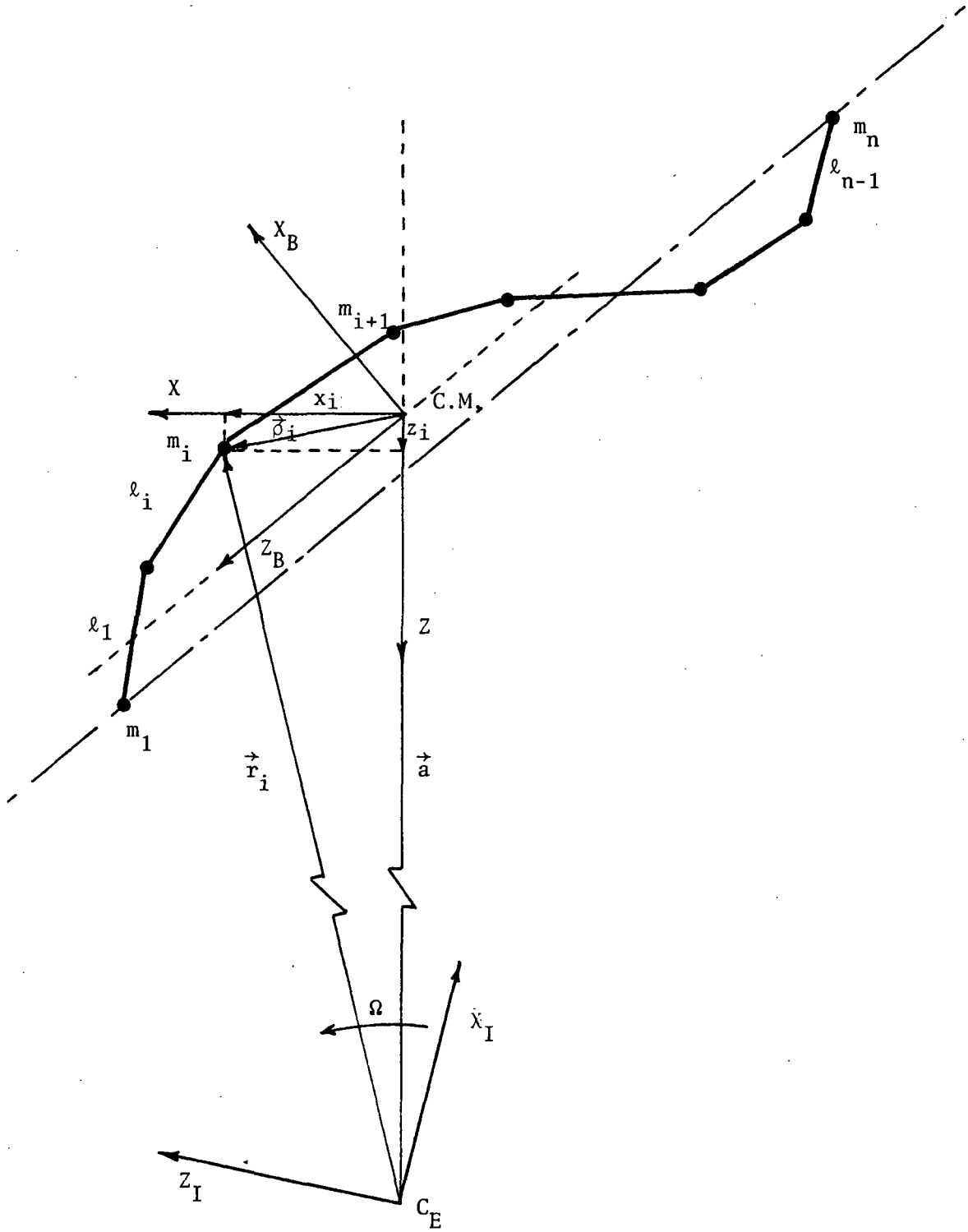
m_n
ℓ_{n-1}
X_B
m_{i+1}
X
x_i
C.M.
$\vec{\rho}_i$
z_i
m_i
ℓ_i
Z_B
ℓ_1
Z
m_1
$\vec{r}_i$
$\vec{a}$
Ω
$\dot{X}_I$
Z_I
C_E

Figure 2.3.1

This equation can also be expressed as:

$$\ddot{\vec{r}}_{Ii} = \ddot{\vec{\rho}}_i + 2\vec{\Omega} \times \dot{\vec{\rho}}_i + \vec{\Omega}\,(\vec{\Omega}\cdot\vec{r}_i) - \vec{r}_i|\vec{\Omega}|^2 \qquad (2.3.4)$$

Since in the two dimensional case $\vec{\Omega}$ is always perpendicular to $\vec{r}_i$ the third term in equation (2.3.4) is equal to zero. By using equations (2.3.2) we finally have:

$$\ddot{\vec{r}}_{Ii} = \left[\ddot{x}_i - 2\Omega\dot{z}_i - \Omega^2 x_i\right]\vec{I} + \left[\ddot{z}_i + 2\Omega\dot{x}_i - \Omega^2\,(z_i - a)\right]\vec{k} \qquad (2.3.5)$$

The equation of motion for the i^{th}-mass is therefore:

$$m_i\ddot{\vec{r}}_{Ii} = \vec{F}_{gi} + \vec{F}_{Ti} + \vec{F}_{pi} \qquad (2.3.6)$$

In equation (2.3.6) $\vec{F}_{gi}$ denotes the gravity force acting upon the i^{th}-mass while $\vec{F}_{Ti}$ is the net force due to tether tension acting upon the same mass and $\vec{F}_{pi}$ is the perturbation force.

Without limiting the generality of the model we assume $\vec{F}_{pi} = 0$. The gravitational force is obtained from the potential energy as follows:

$$\vec{F}_{gi} = -\nabla V_i \qquad (2.3.7)$$

where V_i can be readily derived from equation (2.1.12) obtaining:

$$V_i = \frac{1}{2}\, m_i\left[2\Omega^2 a^2 + 2\Omega^2 a z_i - \Omega^2\,(x_i^2 + z_i^2) + 3\Omega^2 z_i^2\right] \qquad (2.3.8)$$

Substituting in equation (2.3.7) and performing the derivatives we get:

$$\vec{F}_{gi} = m_i\left[(-\Omega^2 x_i)\vec{I} + (\Omega^2 a + 2\Omega^2 z_i)\vec{k}\right] \qquad (2.3.9)$$

The two scalar equations of motion for the i^{th}-mass can be finally written as follows:

$$\begin{aligned} \ddot{x}_i - 2\Omega\,\dot{z}_i &= F_{Txi}/m_i \\ \ddot{z}_i - 3\Omega^2 z_i + 2\Omega\,\dot{x}_i &= F_{Tzi}/m_i \end{aligned} \qquad (2.3.10)$$

These equations are usually called the Hill's equations.

Referring to Figure 2.3.2 the force $\vec{F}_{Ti}$ is given by:

$$\vec{F}_{Ti} = -\left[T_{xi} + T_{x,i-1}\right]\vec{I} - \left[T_{zi} - T_{z,i-1}\right]\vec{k} \qquad (2.3.11)$$

where T_{xi}, T_{zi} are the components of the tension T_i in the tether connecting the i^{th}-mass to the $i+1^{th}$-mass; they are respectively given by:

$$\begin{aligned} T_{xi} &= T_i \cos\beta_i = T_i \frac{x_{i+1} - x_i}{\left[(x_{i+1} + x_i)^2 + (z_{i+1} + z_i)^2\right]^{1/2}} \\ T_{zi} &= T_i \sin\beta_i = T_i \frac{z_{i+1} - z_i}{\left[(x_{i+1} - x_i)^2 + (z_{i+1} - z_i)^2\right]^{1/2}} \end{aligned} \qquad (2.3.12)$$

Referring to Quarterly Report #1 the tension T_i is given by:

$$T_i = \frac{E_i A_i}{\ell_{ci}}\left(\ell_i - \ell_{di} - \ell_{ci}\right) = k_{ti}\,\ell_{ti} \qquad (2.3.13)$$

In equation (2.3.13), ℓ_i is the geometric distance between the i^{th}-mass and the $i+1^{th}$-mass, ℓ_{ci} is the controlled length of that tether segment, ℓ_{di} the length

of the associated longitudinal damper and ℓ_{ti} the tether stretch. The length ℓ_{ci} can follow a prescribed control law if that particular tether segment is actually controlled or it is the tether length at rest if that tether segment is uncontrolled. The length ℓ_{di} is obtained by solving the following equation:

$$\dot{\ell}_{di} = \frac{k_{ti}}{k_{\dot{d}i}} (\ell_i - \ell_{di} - \ell_{ci}) - \frac{k_{di}}{k_{\dot{d}i}} \ell_{di} \qquad (2.3.14)$$

Equation (2.3.14) is the generalization of equation (2.2.5) in Quarterly Report #2. K_{di} and $K_{\dot{d}i}$ are the stiffness and damping coefficient of the i^{th}-longitudinal damper respectively.

We must now derive the expressions that relate the system quantities $(x_1,\ldots,x_n,\ z_1,\ldots,z_n,\ \dot{x}_1,\ldots\dot{x}_n,\ \dot{z}_1,\ldots,\dot{z}_n)$ to the output quantities $(\theta,\ \ell_1,\ldots,\ell_{n-1},\ \epsilon_1,\ldots\epsilon_{n-2},\ \dot{\ell}_1,\ldots,\ \dot{\ell}_{n-1},\ \dot{\epsilon}_1,\ldots,\dot{\epsilon}_{n-2})$. In this report we will derive the expressions that relate the variables while the first derivatives, when necessary, are numerically computed in the computer program. Referring to Figure 2.3.3 we have:

$$\theta = t_g^{-1} \left\{\frac{x_i - x_n}{z_i - z_n}\right\}$$

$$\ell_i = \left[(x_{i+1} - x_i)^2 + (z_{i+1} - z_i)^2\right]^{1/2} \qquad (2.3.15)$$

The lateral displacement ϵ_i is derived by computing the coordinates of the point of intersection between the straight line through m_i and m_n and the straight line perpendicular to it passing through m_i. The equations of the above mentioned lines are respectively given by:

$$z - z_i = \frac{z_n - z_i}{x_n - x_i} (x - x_i)$$

$$z - z_{i+1} = \frac{x_n - x_i}{z_n - z_i} (x - x_{i+1}) \qquad (2.3.16)$$

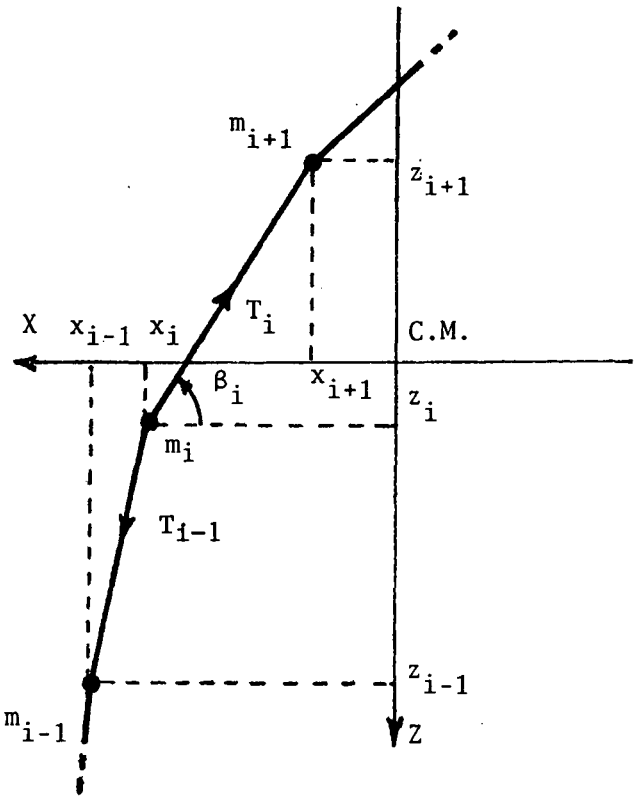

Figure 2.3.2

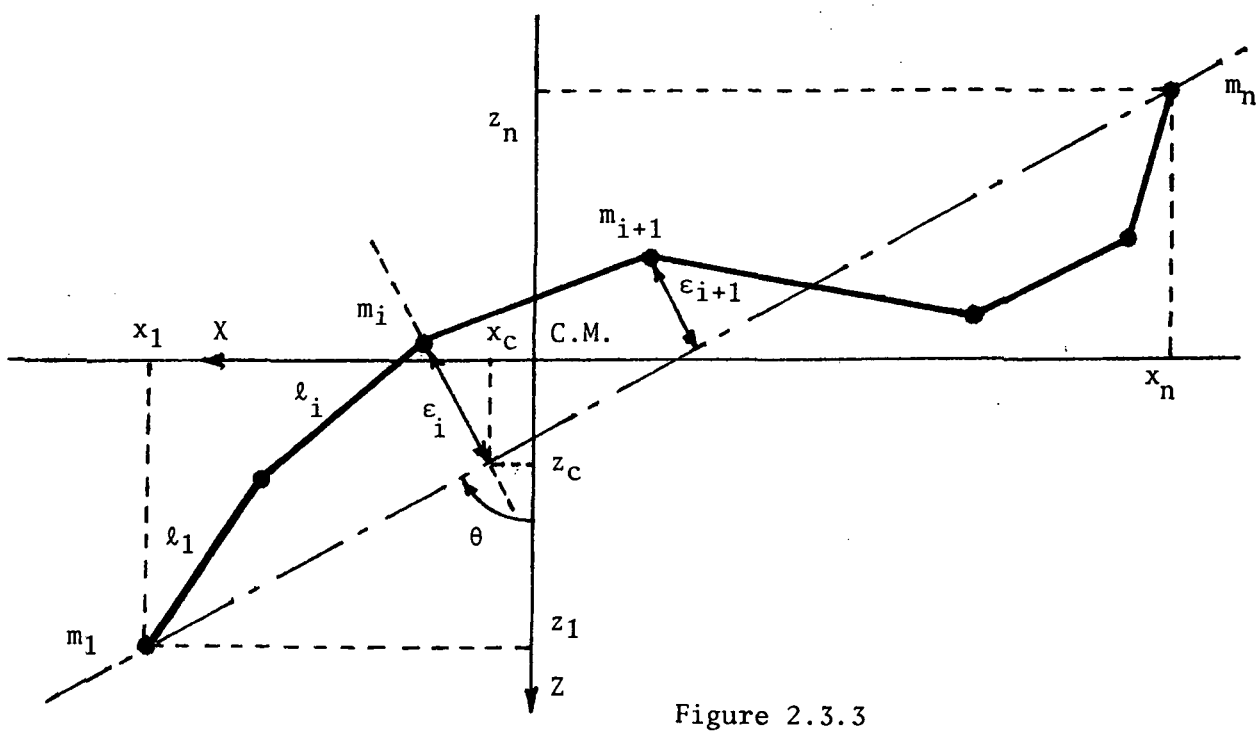

Figure 2.3.3

The solution of equations (2.3.16) are the coordinates of the point of intersection x_{ci}, z_{ci}. After some manipulations we get:

$$x_{ci} = \left[x_1 - x_{i+1}\, t_g^2\theta + (z_{i+1} - z_1)\, t_g\theta\right]/(1 - t_g^2\theta)$$

$$z_{ci} = \left[x_{ci} - x_{i+1}\right] t_g\theta + z_{i+1} \qquad (2.3.17)$$

So that finally ϵ_i is given by:

$$\epsilon_i = \left[(x_{i+1} - x_{ci})^2 + (z_{i+1} - z_{ci})^2\right]^{1/2} \cdot \text{sign}\ (x_{i+1} - x_{ci}) \qquad (2.3.18)$$

Equation (2.3.18) and equations (2.3.17) provide the relations between system variables and output variables.

2.4 The 3-Mass System. Cartesian Coordinate Equations Of Motion

The equations derived in the previous section for an n-mass system are reported, in this section, for a 3-mass system. The equations of motion become as follows:

$$\begin{aligned}
\ddot{x}_1 &= 2\Omega\, \dot{z}_1 + T_1\, (x_2 - x_1)/(m_1\ell_1) \\
\ddot{x}_2 &= 2\Omega\, \dot{z}_2 + T_2\, (x_3 - x_2)/(m_2\ell_2) + T_1 (x_1 - x_2)/(m_2\ell_1) \\
\ddot{x}_3 &= 2\Omega\dot{z}_3 + T_2\, (x_2 - x_3)/(m_3\ell_2) \\
\ddot{z}_1 &= 3\Omega^2 z_1 - 2\Omega\dot{x}_1 + T_1 (z_2 - z_1)/(m_1\ell_1) \\
\ddot{z}_2 &= 3\Omega^2 z_2 - 2\Omega\dot{x}_2 + T_2 (z_3 - z_2)/(m_2\ell_2) + T_1 (z_1 - z_2)/(m_2\ell_1) \\
\ddot{z}_3 &= 3\Omega^2 z_3 - 2\Omega\dot{x}_3 + T_2 (z_2 - z_3)/(m_3\ell_2)
\end{aligned} \qquad (2.4.1)$$

where:

$$
\begin{aligned}
T_1 &= E_1 A_1 \ell_{t1} / \ell_{c1} \\
T_2 &= E_2 A_2 \ell_{t2} / \ell_{c2} \\
\ell_{t1} &= \ell_1 - \ell_{d1} - \ell_{c1} \\
\ell_{t2} &= \ell_2 - \ell_{d2} - \ell_{c2} \\
\dot{\ell}_{d1} &= k_{t1} \ell_{t1} / k_{\dot{d}1} - k_{d1} \ell_{d1} / k_{\dot{d}1} \\
\dot{\ell}_{d2} &= k_{t2} \ell_{t2} / k_{d2} - k_{d2} \ell_{d2} / k_{\dot{d}2}
\end{aligned}
\qquad (2.4.2)
$$

The relations between system variables and output variables become:

$$
\begin{aligned}
\theta &= tg^{-1}\left[(x_1 - x_3) / (z_1 - z_3) \right] \\
\ell_1 &= \left[(x_2 - x_1)^2 + (z_2 - z_1)^2 \right]^{1/2} \\
\ell_2 &= \left[(x_3 - x_2)^2 + (z_3 - z_2)^2 \right]^{1/2} \\
\epsilon_1 &= \left[(x_2 - x_{c1})^2 + (z_2 - z_{c1})^2 \right]^{1/2} \cdot \operatorname{sign}(x_2 - x_{c1})
\end{aligned}
\qquad (2.4.3)
$$

where:

$$
\begin{aligned}
x_{c1} &= \left[x_1 - x_2 tg^2\theta + (z_2 - z_1) tg\theta \right] / (1 - tg^2\theta) \\
z_{c1} &= \left[x_{c1} - x_2 \right] tg\theta + z_2
\end{aligned}
\qquad (2.4.4)
$$

Equations (2.4.1) through (2.4.4) have been numerically integrated in a newly developed computer code to obtain the results illustrated in the following sections.

2.5 Generating Sinusoidal Acceleration Profiles

A unique feature of a 3-mass, vertical, tethered system is the capability of providing a variable-g level in the middle platform by simply moving the platform along the tether. The middle platform experiences a vertical acceleration, linearly dependent upon the distance from the system C.M., given in g-unit by the following formula:

$$a_v = 9.81 \times 3\Omega^2 \ell_{C.M.} \qquad (2.5.1)$$

By controlling the distance $\ell_{C.M.}$ it is possible, in principle, to produce a desired vertical acceleration profile. Actually the scenario is more complex: any displacement of the middle mass from a rest condition generates a transient response of the tethered system. Namely, the motion of the middle mass induces longitudinal oscillations of the elastic tethers and its non-zero velocity interacts with the orbital rate producing a Coriolis force that deflects, away from the vertical, the acceleration measured at the middle platform. During the acceleration or deceleration phase, moreover, the non-zero acceleration of the platform is added to the gravity gradient acceleration. The acceleration profile obtained is therefore a result of many parameters, its departure from the nominal profile depending primarily upon the control laws adopted and the effectiveness of the dampers.

The first case that we analyze is the generation of sinusoidal acceleration profiles with the middle mass starting from the system C.M. and moving in between the upper end mass and the initial C.M. position. The Space Station mass adopted in the following simulations is consistent with the post-IOC phase of the Space Station program. The other parameters of the micro-g/variable-g labo-

ratory are not intended to be definitive: they provide a possible configuration of the system that is not based upon optimization criteria. The system parameters are as follows:

Space Station Mass (m_1):	3.06752×10^5 kg	
Middle Mass (m_2):	5×10^3 kg	
End Mass (m_3):	10^4 kg	(2.5.2)
Tether Length:	10 km	
Orbital Height at the System C.M.:	450 km	

The tether is a 2. mm diameter kevlar tether. In these particular simulations the longitudinal dampers are non-adaptative; they are tuned respectively to the longitudinal frequency of the associated tether segments at their initial tether length. The angular frequenices are given by:

$$\omega_{\ell 1} = \sqrt{EA/(\ell_{c10} m_1)}$$

$$\omega_{\ell 2} = \sqrt{E\ A/(\ell_{c20} m_2)} \qquad (2.5.3)$$

where ℓ_{c10} and ℓ_{c20} are the initial, controlled tether lengths for tether #1 and tether #2 respectively. The damping coefficient in both the longitudinal dampers is assumed equal to .9. The rotational (θ) and lateral (ϵ) active damping algorithms are operated according to the description given in section 2.3 and 2.4 of Quarterly Report #2.

The control laws adopted for the sinusoidal acceleration variation are as follows:

$$\ell_{c1} = \ell_{c10} + \Delta\ell_c \left[1 + \sin\ (\omega_c t + \frac{3}{2}\pi)\right]$$

$$\ell_{c2} = \ell_{c20} - \Delta\ell_c \left[1 + \sin\ (\omega_c t + \frac{3}{2}\pi)\right] \qquad (2.5.4)$$

In equations (2.5.4) $\Delta\ell_c$ is the amplitude of the sinusoidal displacement so that the peak-to-peak displacement is $2\Delta\ell_c$ and ω_c is the angular frequency. Neglecting effects such as tether elasticity and lateral displacement of the mass m_2, the resulting vertical acceleration measured at the middle platform, in zero order approximation, is given by:

$$a_v = 3\Omega^2 \ell_{C.M.} - \Delta\ell_c \omega_c^2 \sin\ (\omega_c t + \frac{3}{2}\pi) \qquad (2.5.5)$$

Assuming that the position of the C.M. does not move appreciably during the motion of the middle platform (as is the case in zero order approximation) we have:

$$\ell_{C.M.} \simeq \Delta\ell_c \left[1 + \sin\ (\omega_c t + \frac{3}{2}\pi)\right] \qquad (2.5.6)$$

Finally we get:

$$a_v = 3\Omega^2 \Delta\ell_c + \Delta\ell_c\ (3\Omega^2 - \omega_c^2)\ \sin\ (\omega_c t + \frac{3}{2}\pi) \qquad (2.5.7)$$

The resulting vertical acceleration variation is therefore dependent upon both Ω and ω_c. The point of zero acceleration is no longer the system C.M. but occurs according to the following formula:

$$\omega_c t = \sin^{-1}\left[1/(\omega_c/3\Omega^2 - 1)\right] - \frac{3}{2}\pi + k2\pi \qquad k = 1, 2, \ldots \qquad (2.5.8)$$

If $\omega_c < \Omega$ then the second term in equation (2.5.5) is negligible. Since the effects of tether elasticity and Coriolis acceleration are also smaller for low values of ω_c, the resulting acceleration variations of m_2 are closer to nominal.

In the following set of simulations we assume $\omega_c = 10^{-3}$ rad/sec while the effect of a different amplitude $\Delta\ell_c$ is explored. The first group of plots shown in Figure 2.5.1 a-l is relevant to a peak-to-peak displacement $2\Delta\ell_c = 2000$ m. All the dampers are active. The simulation has been run for 11000 sec which is approximately 2 orbits. Figure 2.5.1a shows the sinusoidal length variation of tether #1 vs. time. Figure 2.5.1b represents the longitudinal damper length variation for the same tether. Figure 2.5.1c is the in-plane (θ) angle vs. time while Figure 2.5.1d is the phase plane θ-$\dot{\theta}$. Figure 2.5.1e is the phase plane ϵ-$\dot{\epsilon}$ where ϵ is the lateral displacement of m_2 from the line through m_1 and m_3. These last two figures show that the tethered system, after dissipating the initial transient motion, follows a steady state limit cycle sustained by the motion of m_2. Figure 2.5.1f shows the components of the acceleration measured at the middle platform. The vertical component (a_v) is sinusoidal in shape but, as mentioned before, the zero-g acceleration point is no longer at the crossing of the system C.M. Because of the middle mass self acceleration the vertical component (a_v) overshoots towards the positive values (acceleration directed downwards). Note also that a much smaller, but not negligible, horizontal component (a_h) appears. It is related to the Coriolis force. Figure 2.5.1g is an isometric, polar diagram of the acceleration. The vector connecting the 0,0 point to any point along the curve gives the actual orientation and modulus of the acceleration. After the transient phase is over the acceleration vector rotates steadily around the C.M. of the middle platform at the angular frequency ω_c. Figure 2.5.1h is the isometric side view trajectory of the middle mass with respect to the system C.M. Negative numbers in the z axis meaning upwards. For

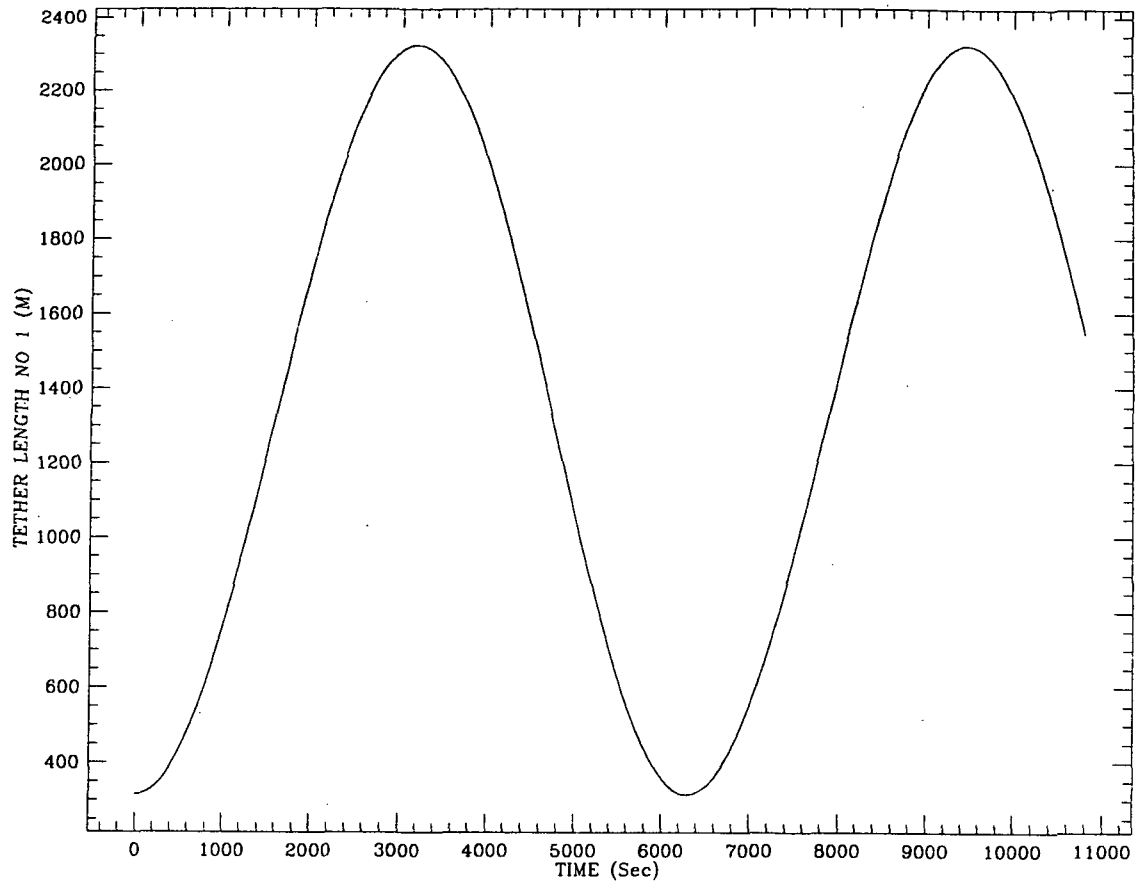

Figure 2.5.1a

Figure 2.5.1b

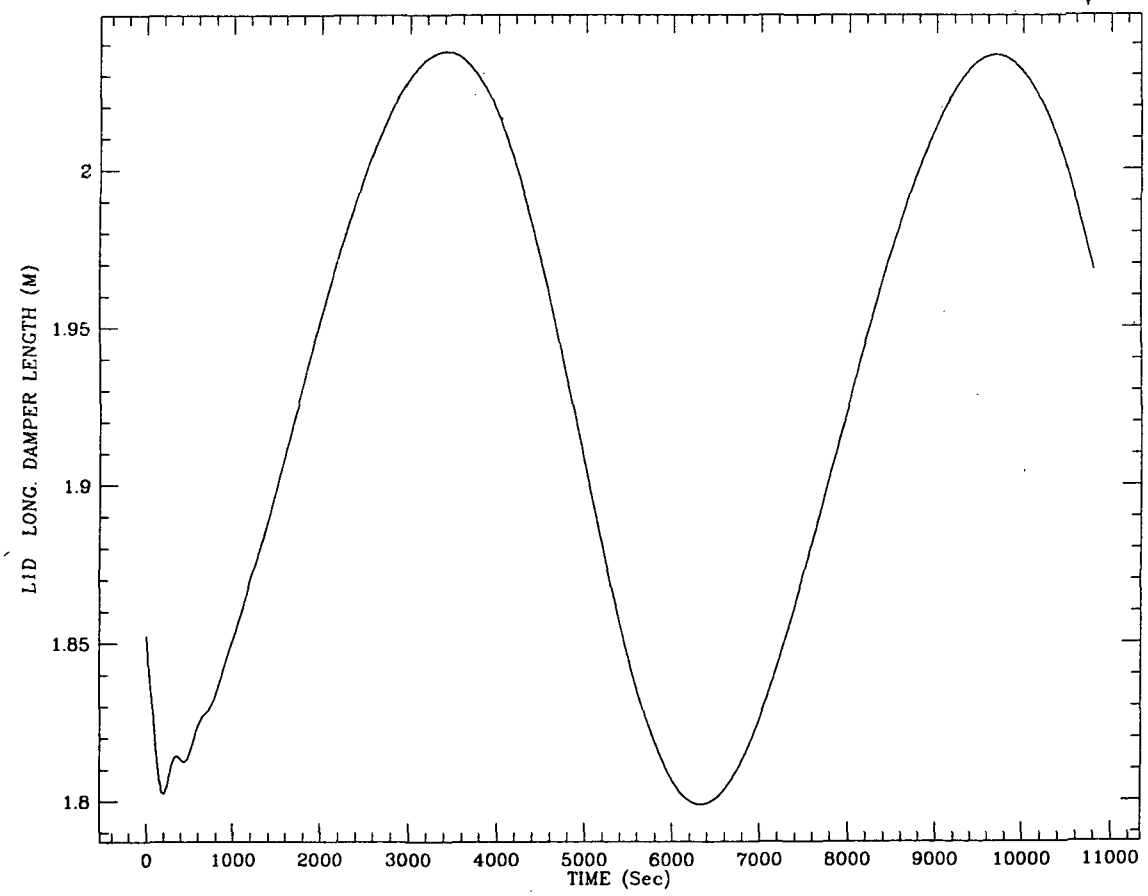

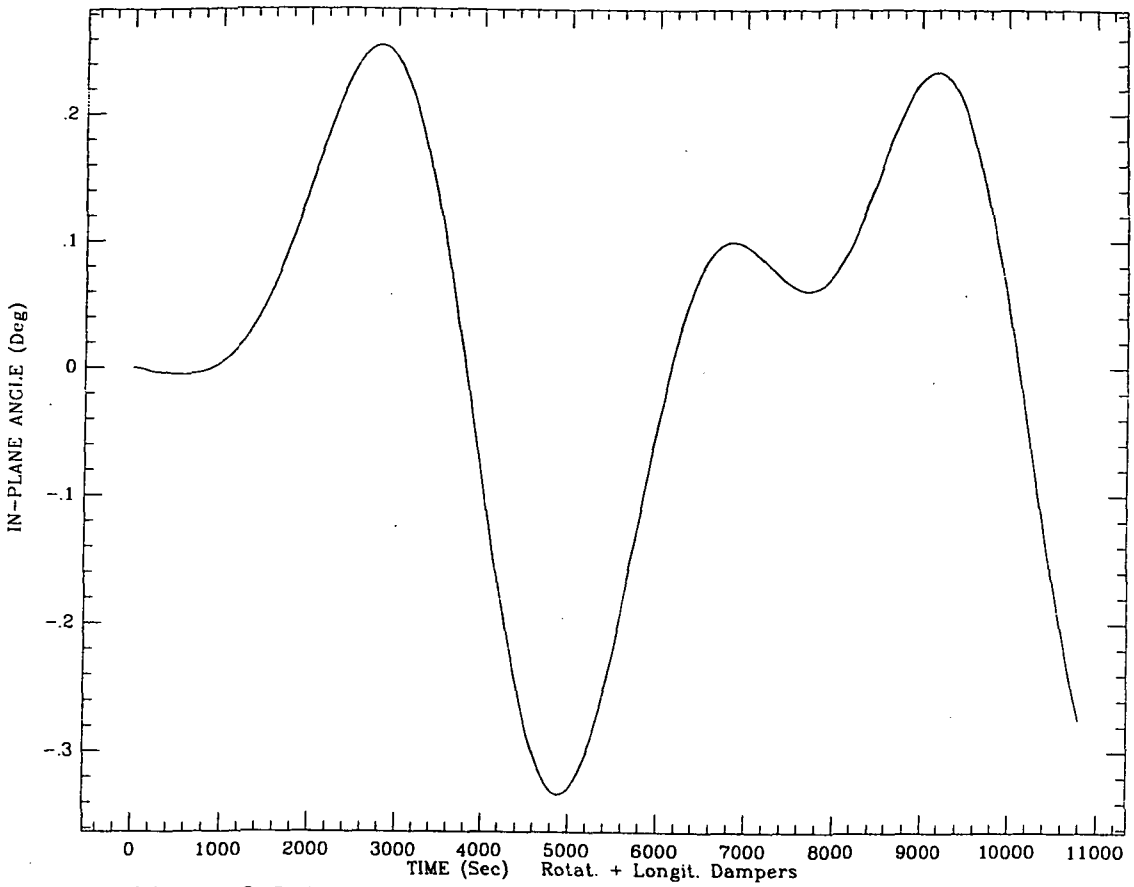

Figure 2.5.1c↑

Figure 2.5.1d↓

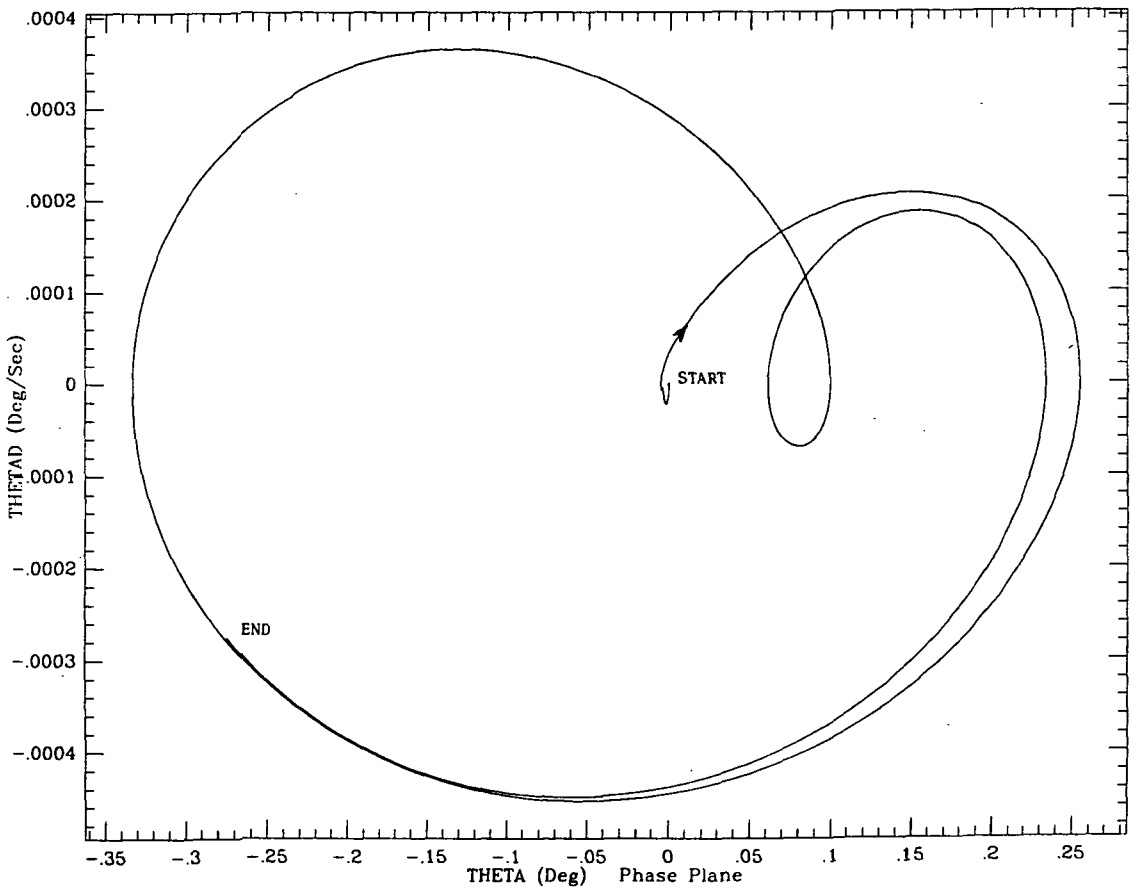

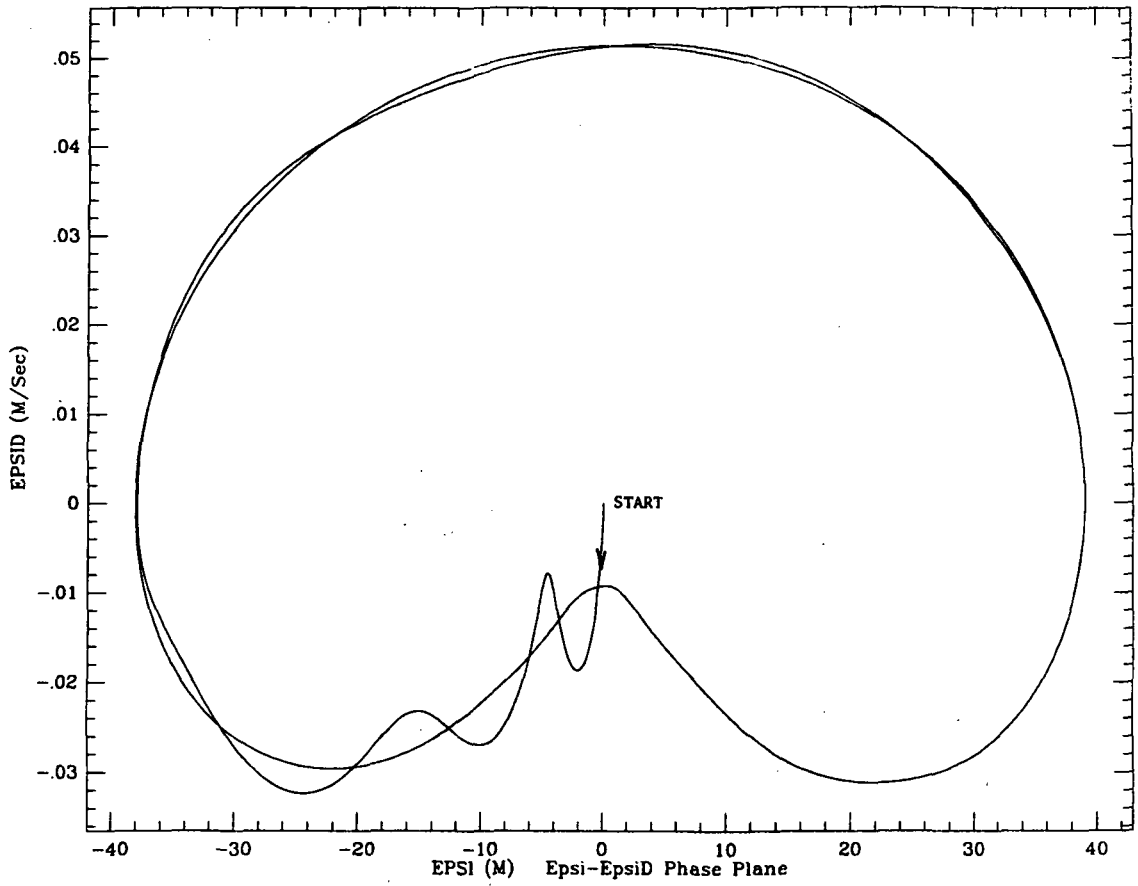

Figure 2.5.1e

Figure 2.5.1f

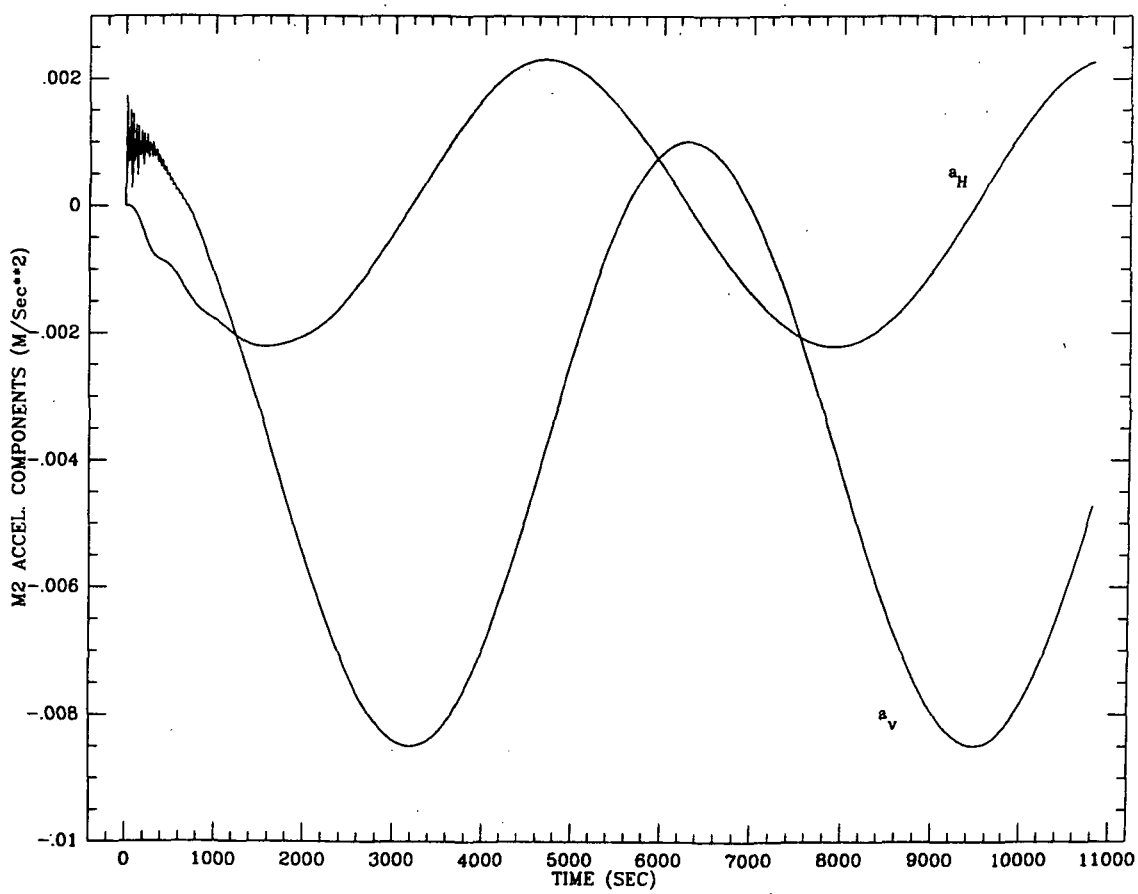

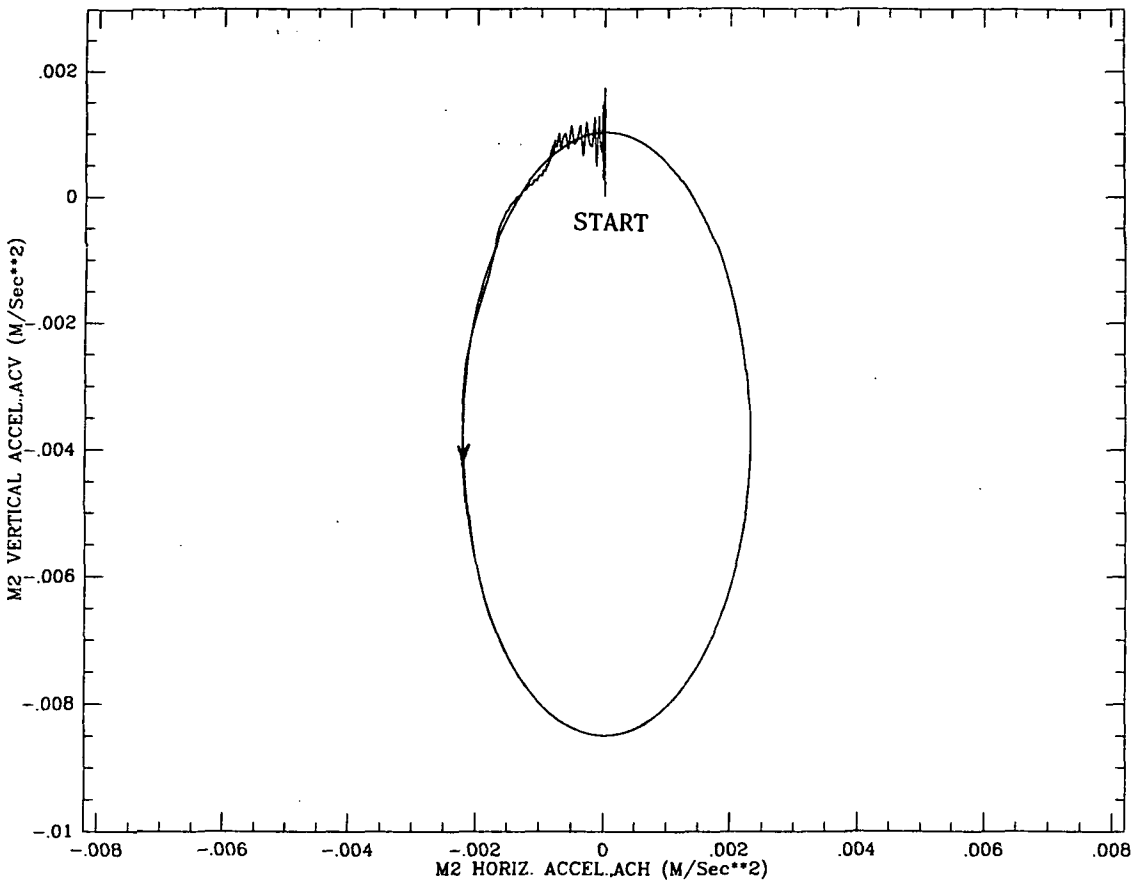

Figure 2.5.1g

Figure 2.5.1h

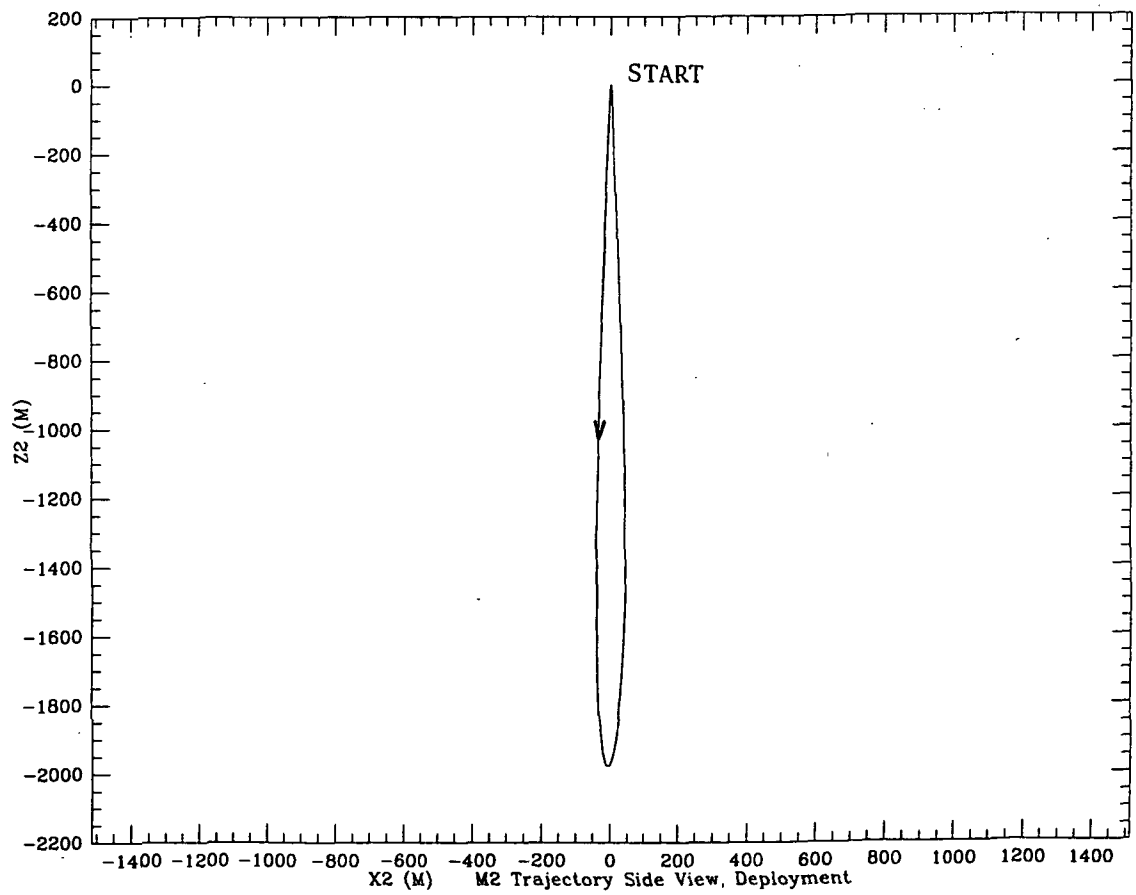

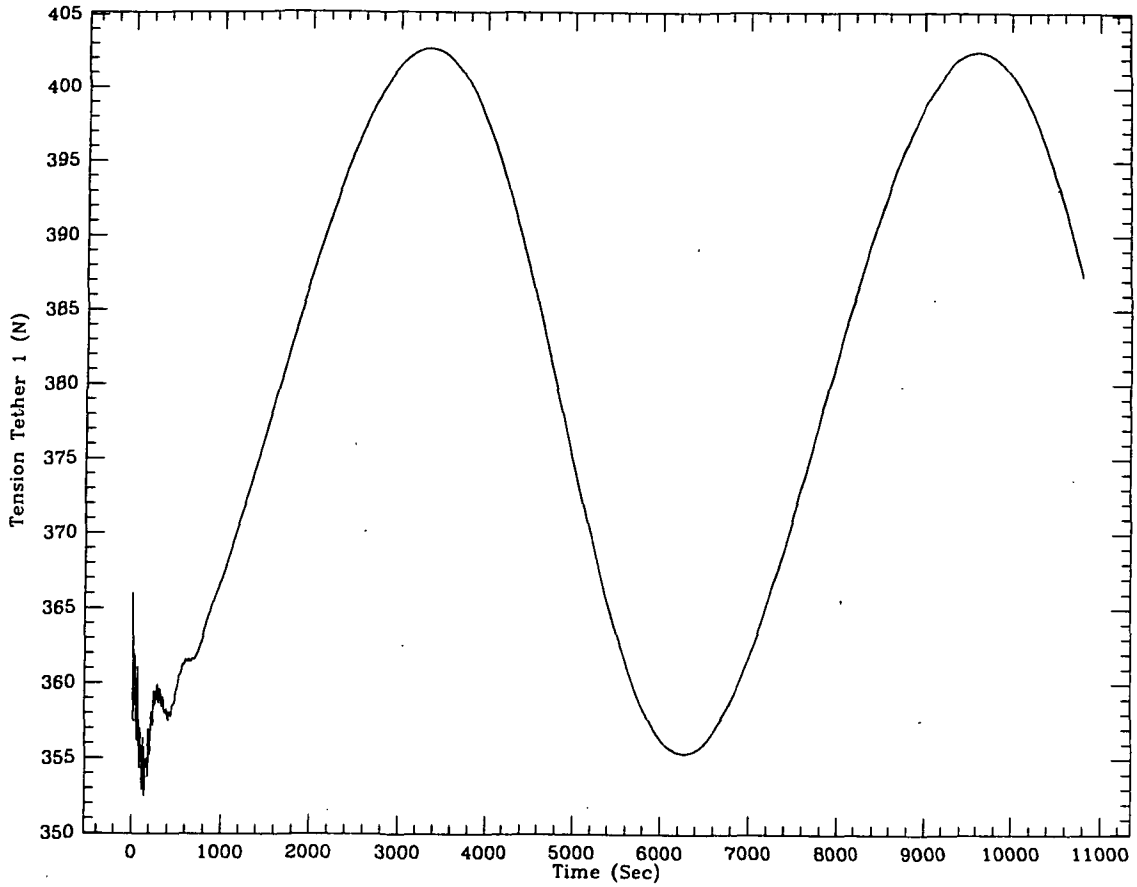

Figure 2.5.1i

Figure 2.5.1l

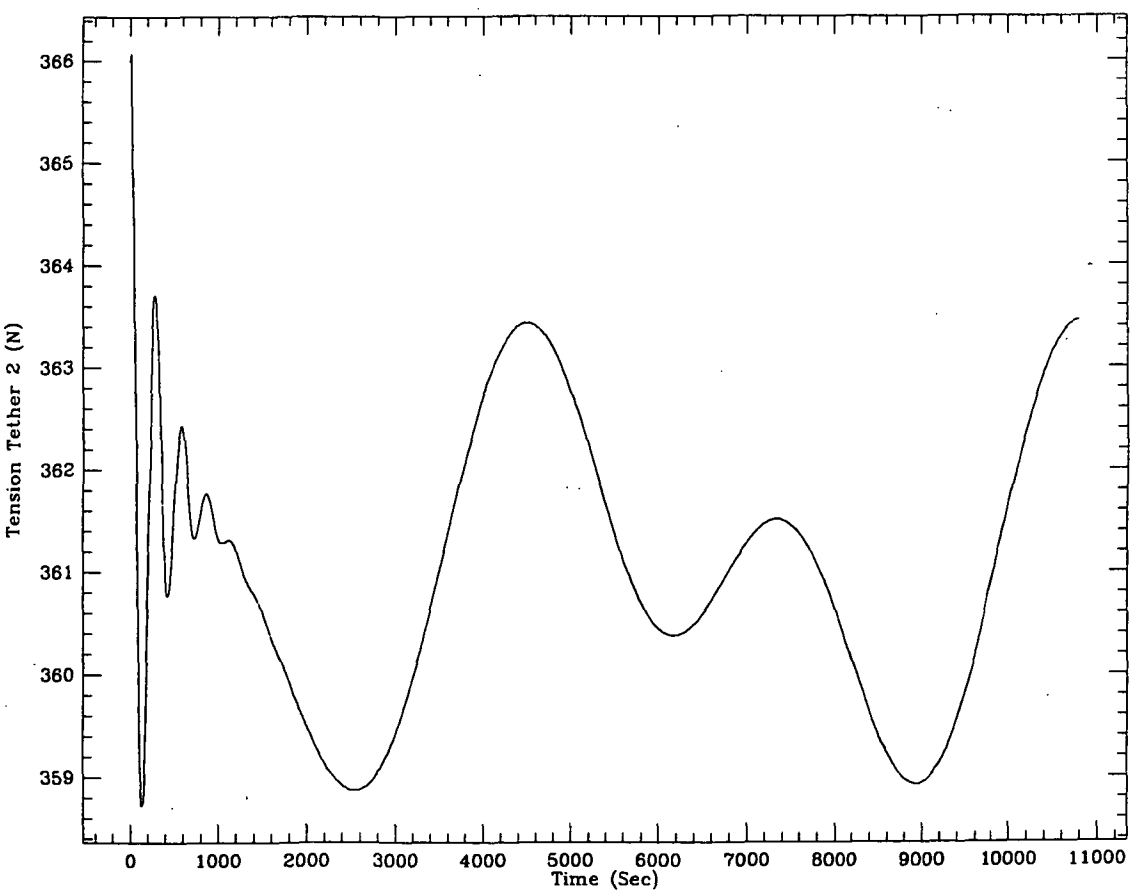

completeness Figures 2.5.1 i and l show the tension in tethers #1 and #2 respectively.

A second case with a peak-to-peak tether length equal to 8000m is shown in Figure 2.5.2 a-l. Comments similar to those for Figure 2.5.1 hold true in this case. The shape of the trajectory side view of mass m_2 is less symmetrical with respect to the local vertical; in general, however, the behavior is qualitatively very similar to the previous case. Quantitatively the acceleration components show a dependence with $\Delta\ell_c$ so that they are 4 times bigger than in the previous simulation.

2.6 G-Tuning

The possibility of varying the acceleration level in the middle platform provides a "g-tuning" capability. This means that the middle platform is moved from the zero-g point of the tethered system and is placed at the appropriate distance in order to have the requested g-level according to equation (2.5.1). Two different control laws are shown here. They are both open loop control laws in the sense that the acceleration in the middle mass is not fed back into the control system. The final acceleration value, therefore, depends only upon the final distance ($\ell_{C.M.}$) achieved. The first control law adopted is a sinusoidal control law, similar to the one illustrated in the previous section, that has been truncated after half a cycle. In Figure 2.6.1a-m the dynamic response of the system is shown in a case with a peak-to-peak displacement of the middle platform equal to 2000 m. Figure 2.6.1a depicts the tether length for tether #1 vs. time: the sinusoidal control law is clearly visible. Figure 2.6.1b is the length variation of the longitudinal damper. Further comments on the figure

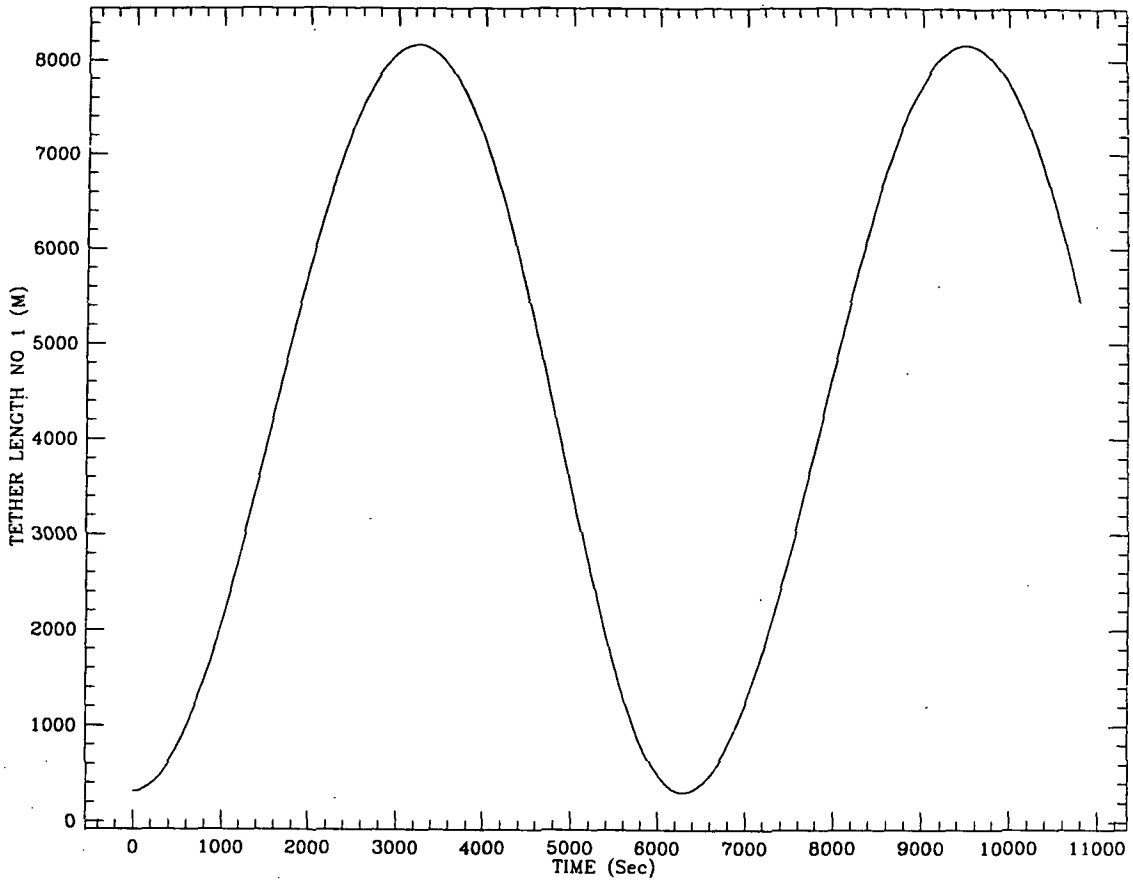

Figure 2.5.2a

Figure 2.5.2b

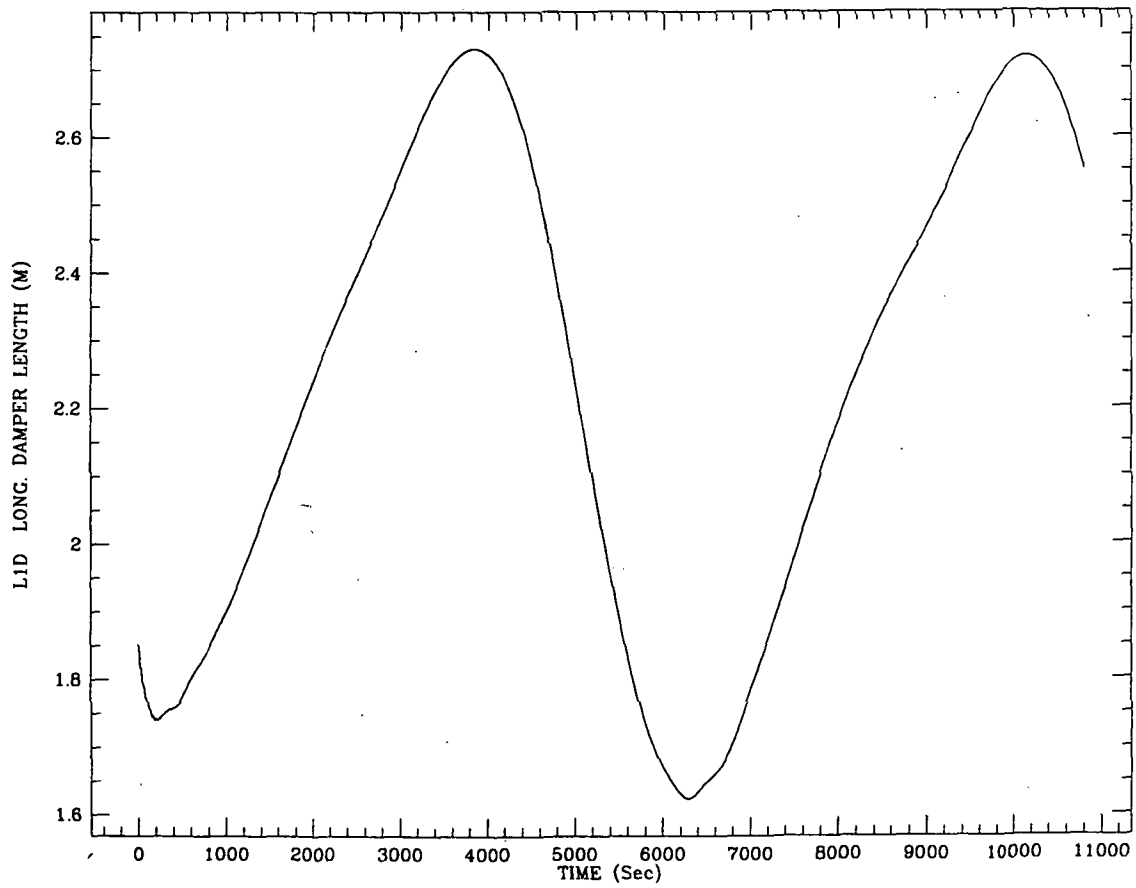

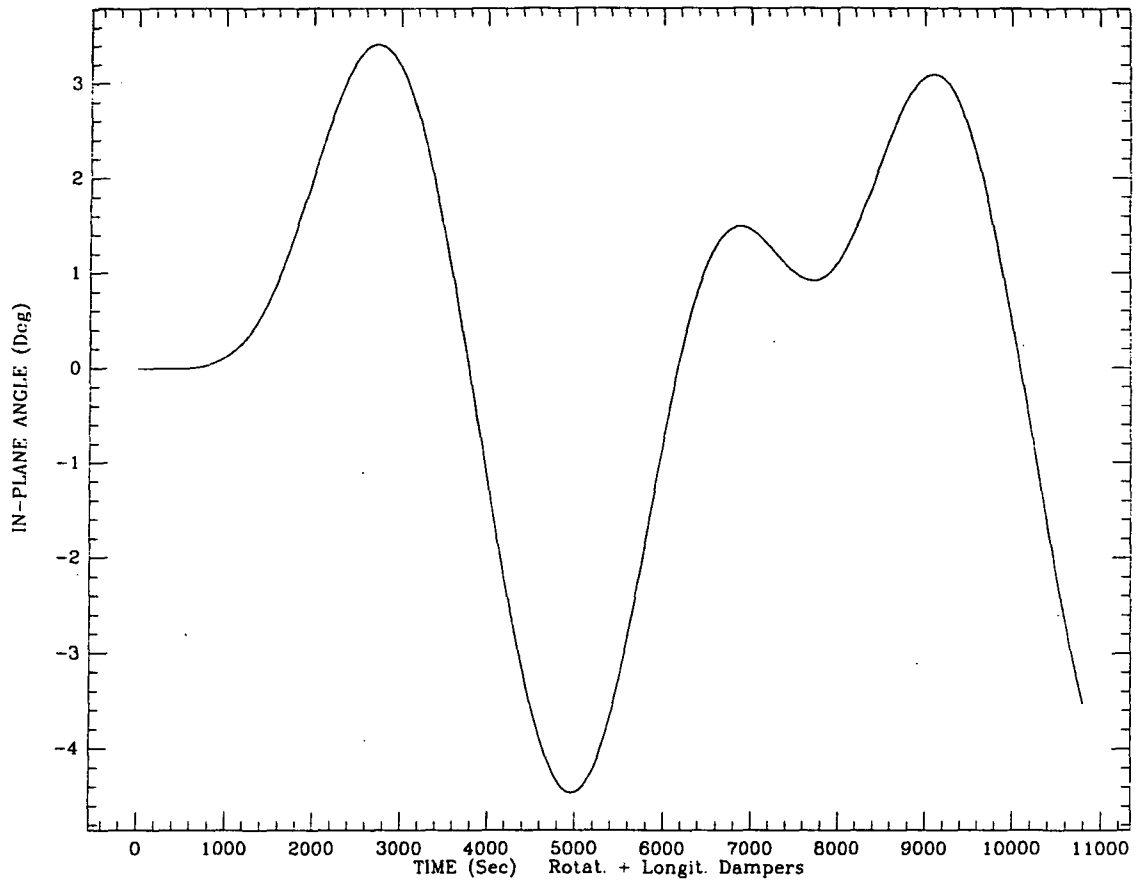

Figure 2.5.2c↑

Figure 2.5.2d↓

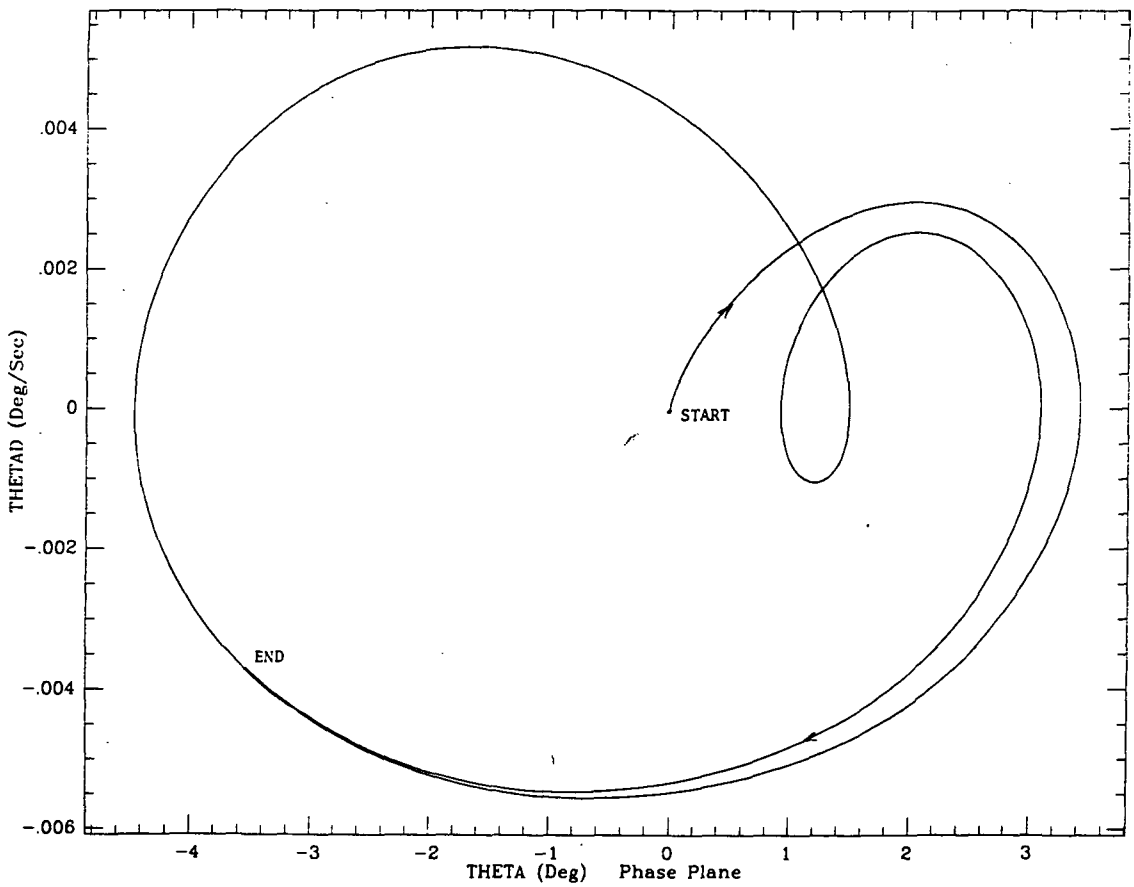

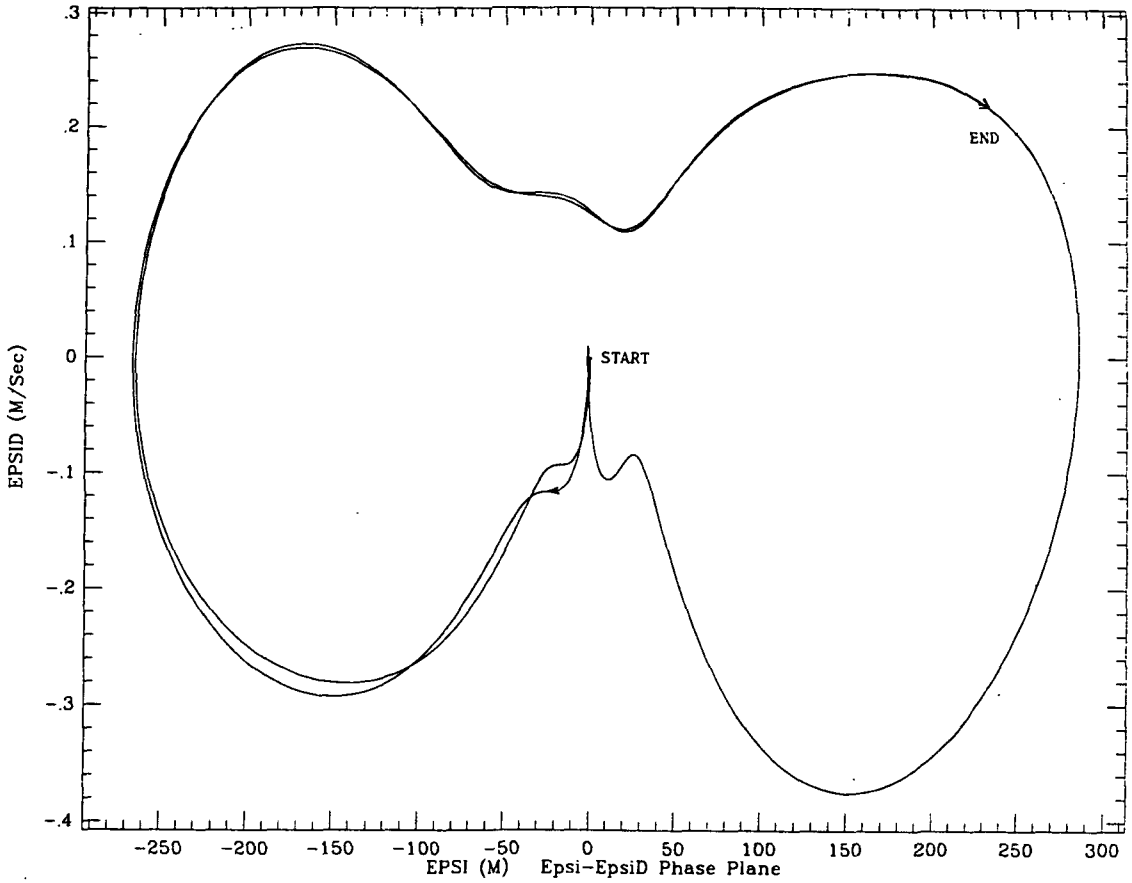

Figure 2.5.2e↑

Figure 2.5.2f↓

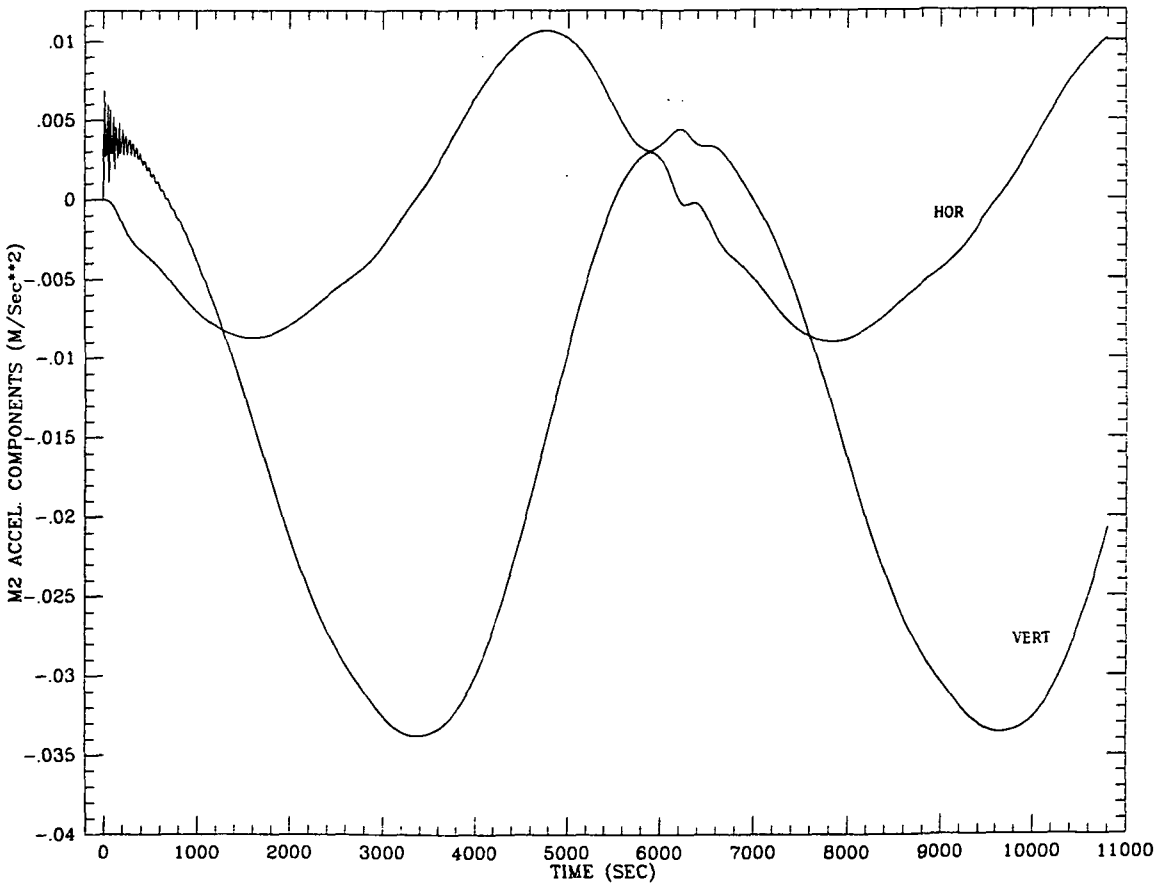

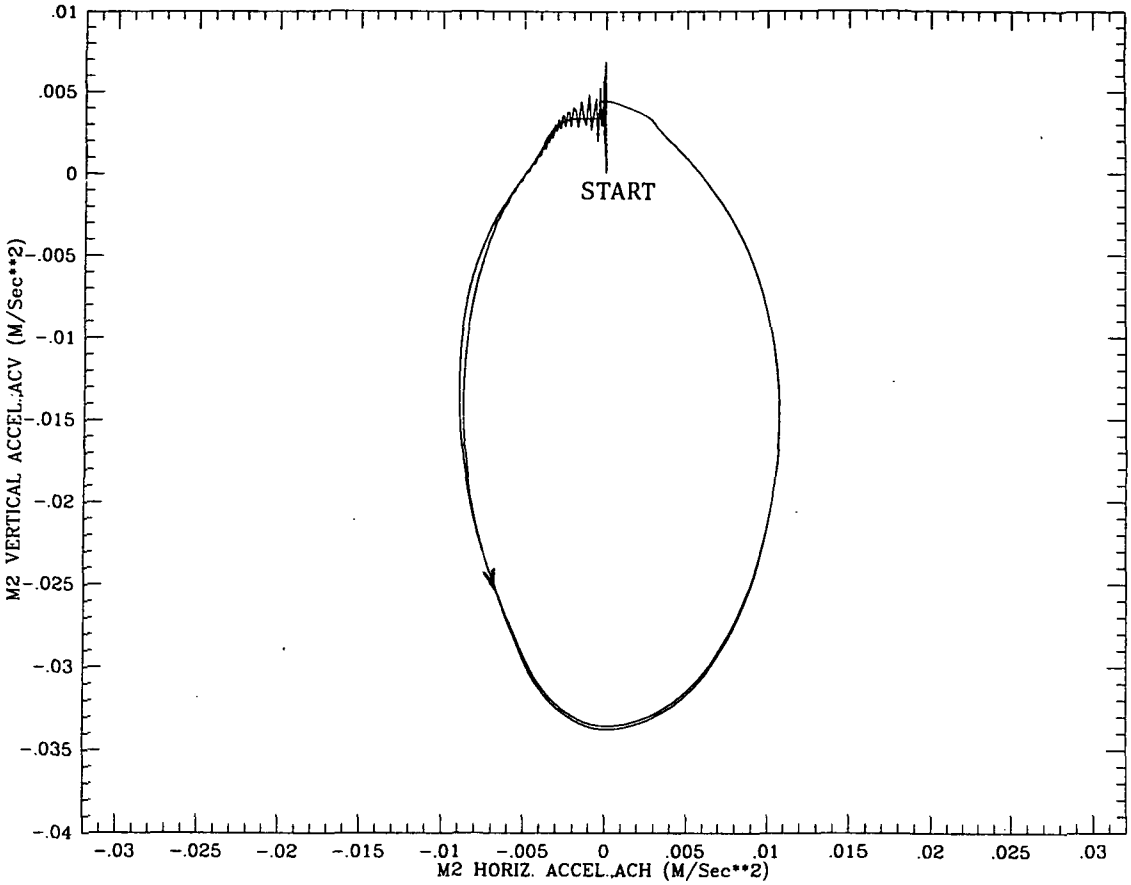

Figure 2.5.2g↑

Figure 2.5.2h↓

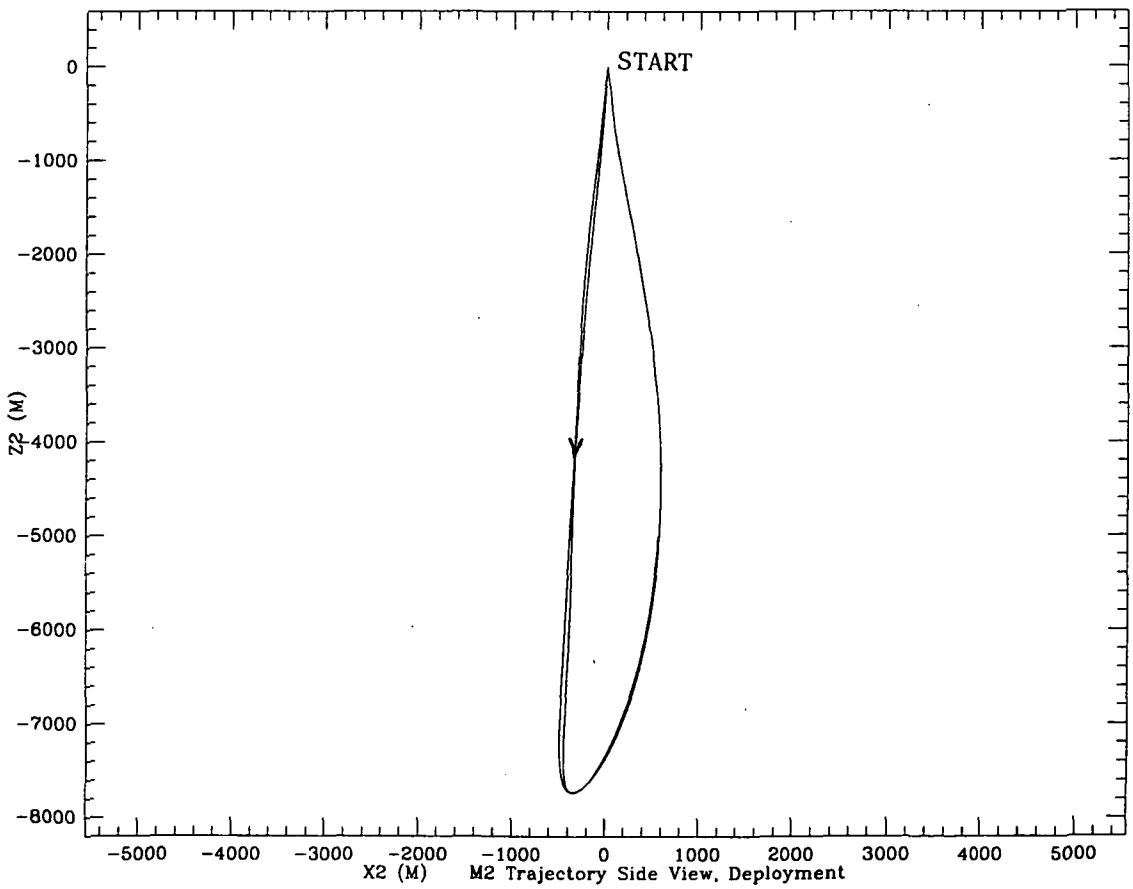

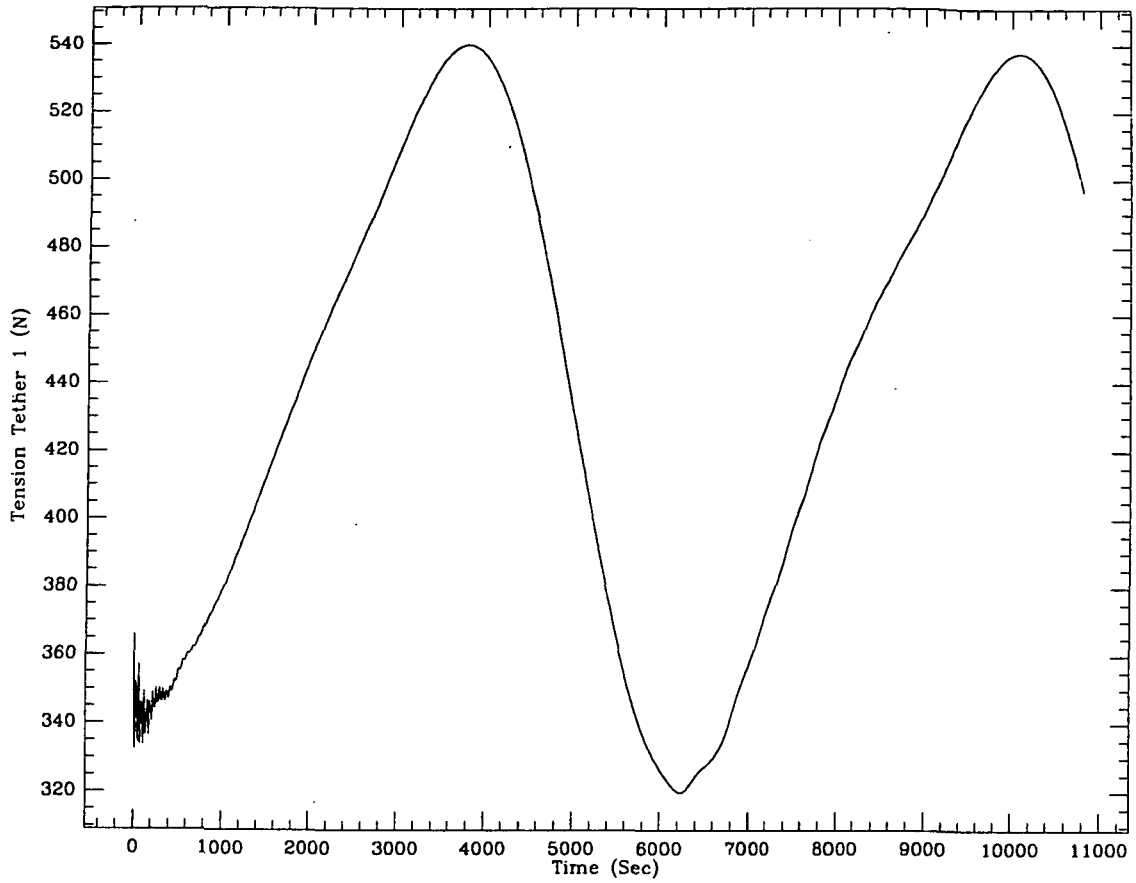

Figure 2.5.2i↑

Figure 2.5.2ℓ↓

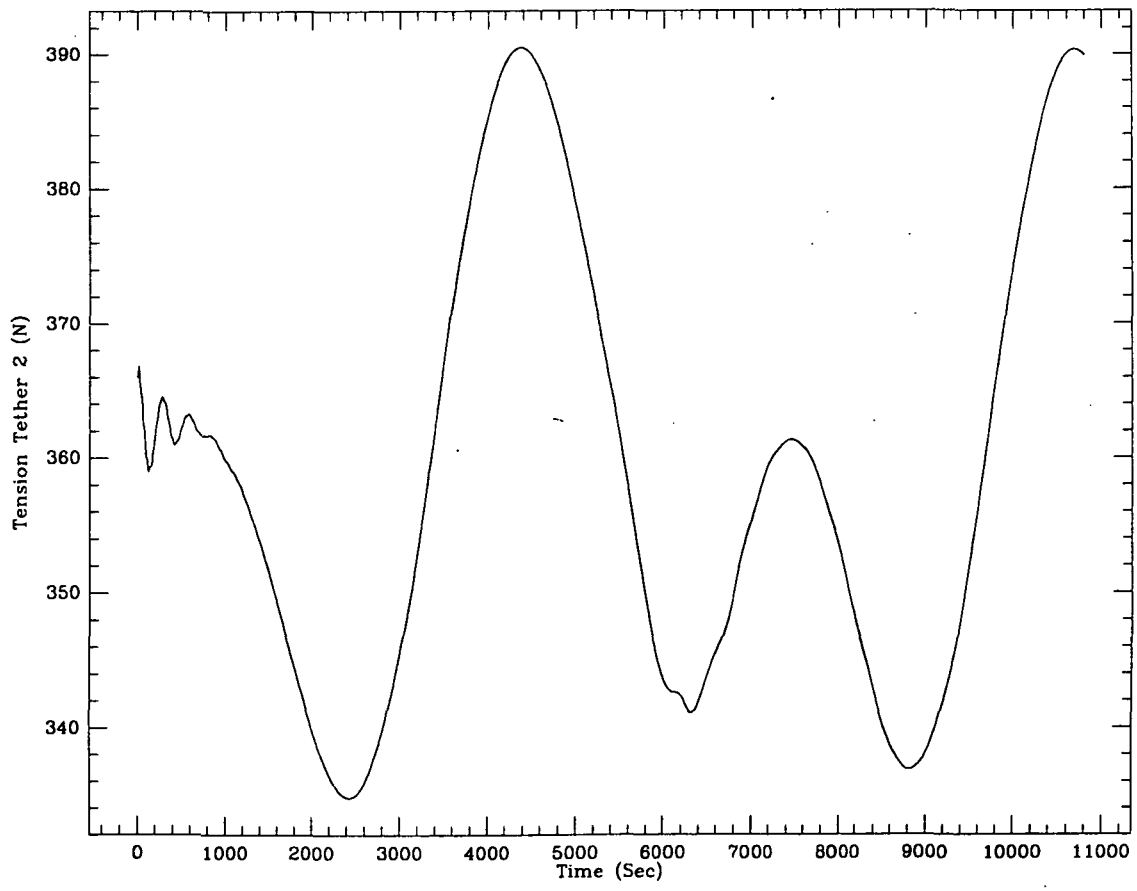

will be provided later on. Figures 2.6.1c and d are the in-plane angle vs. time and the phase plane θ-$\dot{\theta}$ respectively. These two figures show that after 7200 sec there is still a small residual in-plane oscillation decreasing to zero. Similar comments are applicable to Figure 2.6.1e and f which represent the lateral deflection ϵ and the phase plane ϵ-$\dot{\epsilon}$ respectively. Figure 2.6.1g shows the acceleration components, along the orbiting reference frame, measured at the middle mass. In this "g-tuning" simulation the horizontal component disappears after the transient phase is over. The vertical component is however experiencing a steep variation at the time when the final distance from the C.M. has been reached because of the non-zero acceleration provided by the control law at that point. This effect accounts for the similar steep variation in the longitudinal damper's length. The system, therefore, needs additional time to reach a steady state acceleration condition. Figure 2.6.1h shows the isometric, polar diagram of the acceleration; it stresses again the negative effect of using a control law (sinusoidal) that has non-zero acceleration at the beginning and at the end. Figure 2.6.1i is an isometric plot of the trajectory side view of mass m_2 with the zero point located at the initial position of the system C.M. Figure 2.6.1ℓ and m show the tension in tether #1 and tether #2 respectively. The larger oscillations in tether #2 tension are due to the expanded plotting scale. The results obtained by using the sinusoidal control law for "g-tuning" prompted us to adopt a control law with zero acceleration at the end of the maneuver. The new control law is a modified hyperbolic tangent; the tether lengths are controlled according to:

$$\ell_1 = \ell_{10} + \Delta\ell_c \ (1 - e^{-\beta t}) \ \tanh(\alpha t)$$

$$\ell_2 = \ell_{20} - \Delta\ell_c \ (1 - e^{-\beta t}) \ \tanh(\alpha t) \qquad (2.6.1)$$

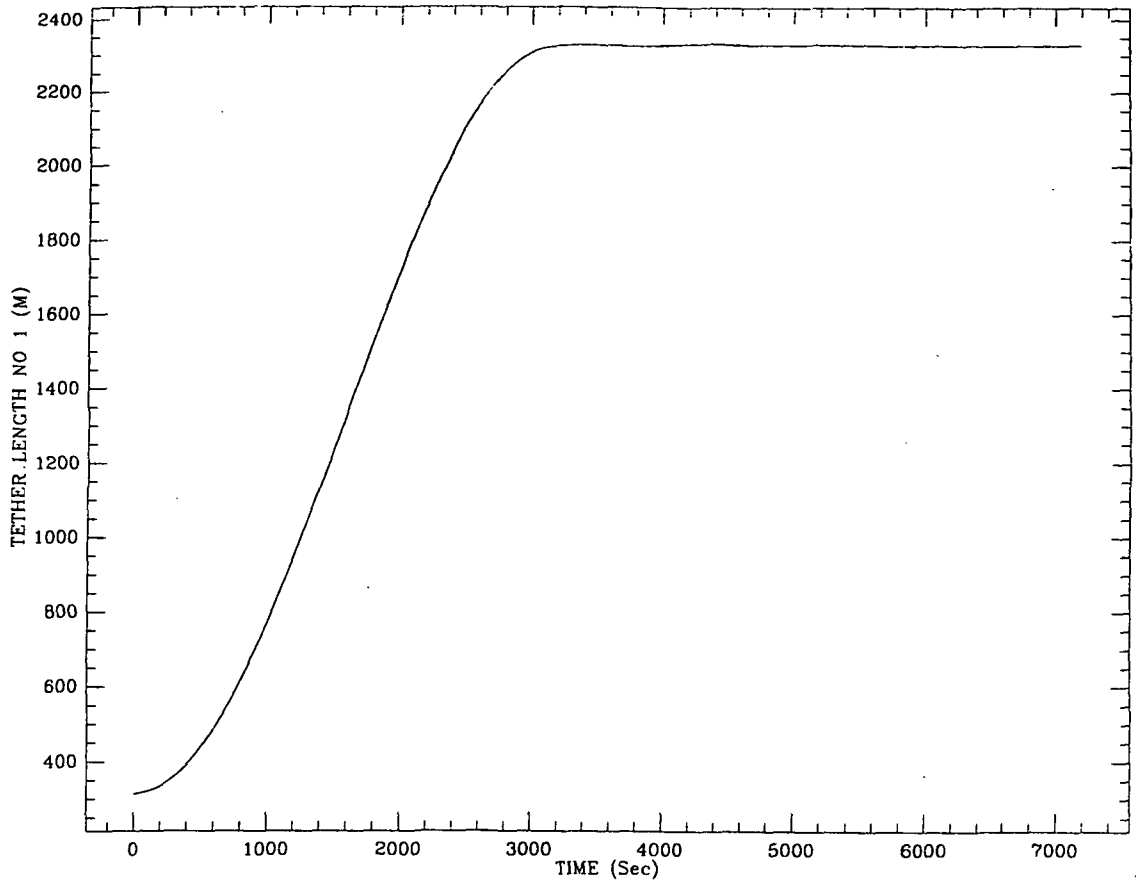

Figure 2.6.1a

Figure 2.6.1b

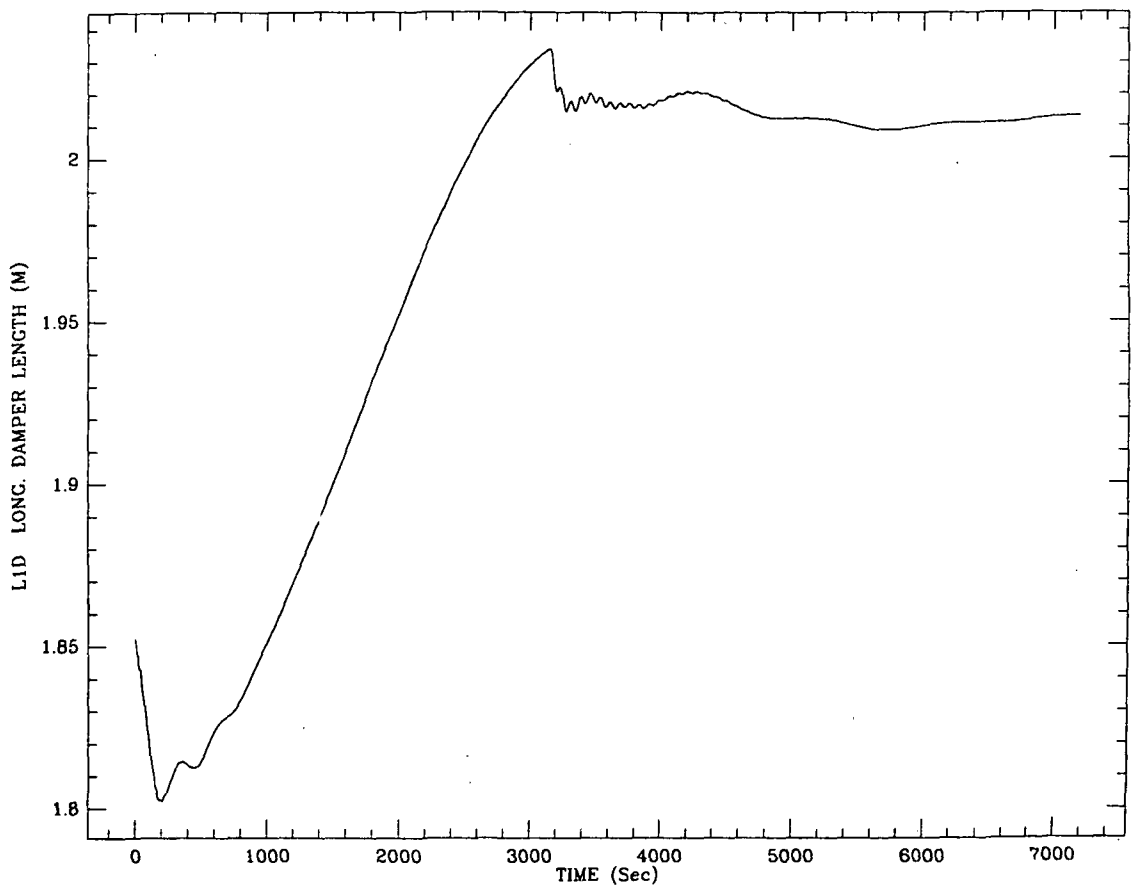

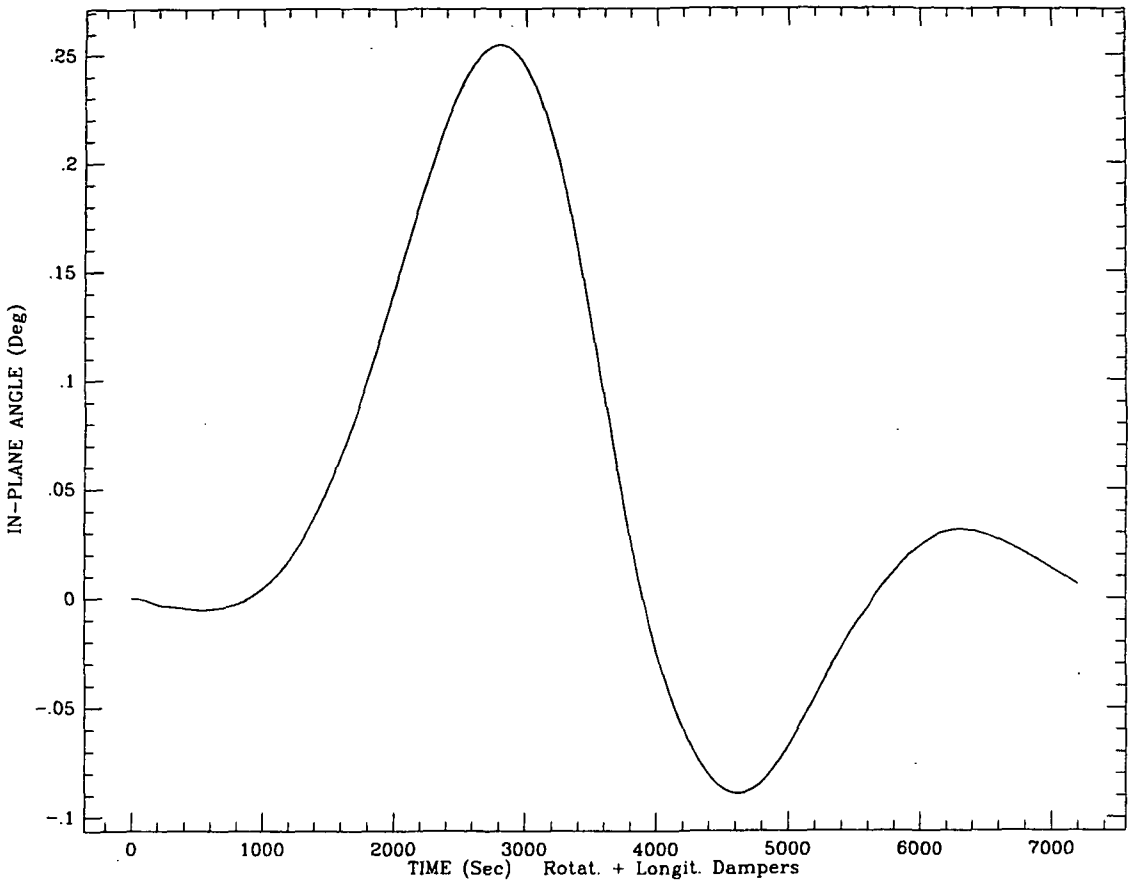

Figure 2.6.1c↑

Figure 2.6.1d↓

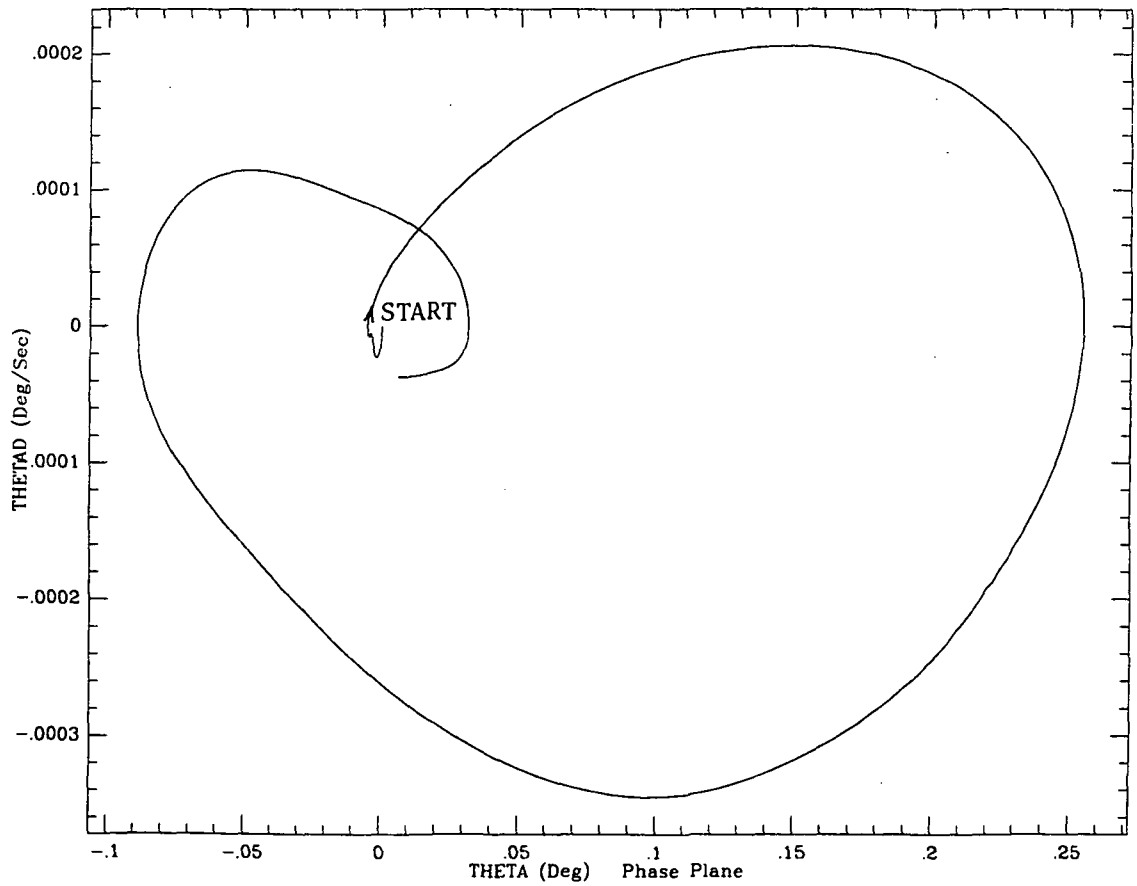

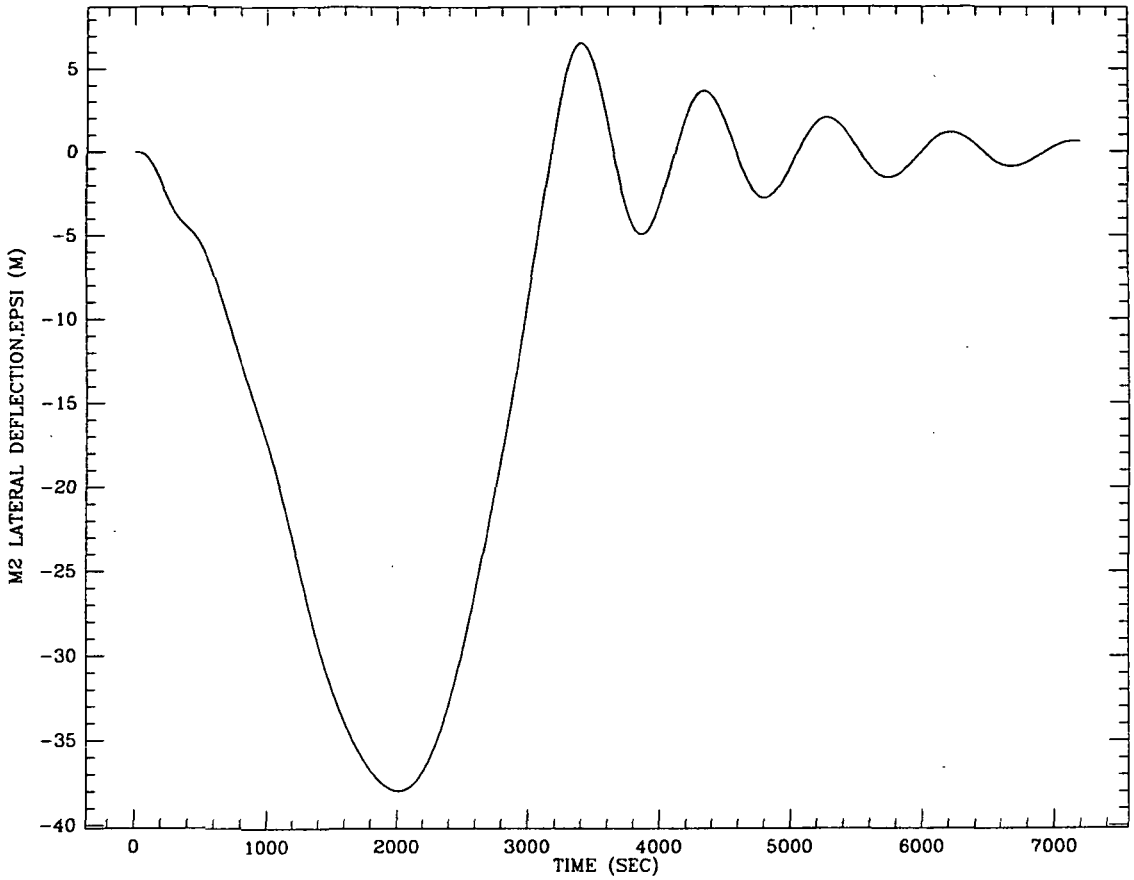

Figure 2.6.1e↑

Figure 2.6.1f↓

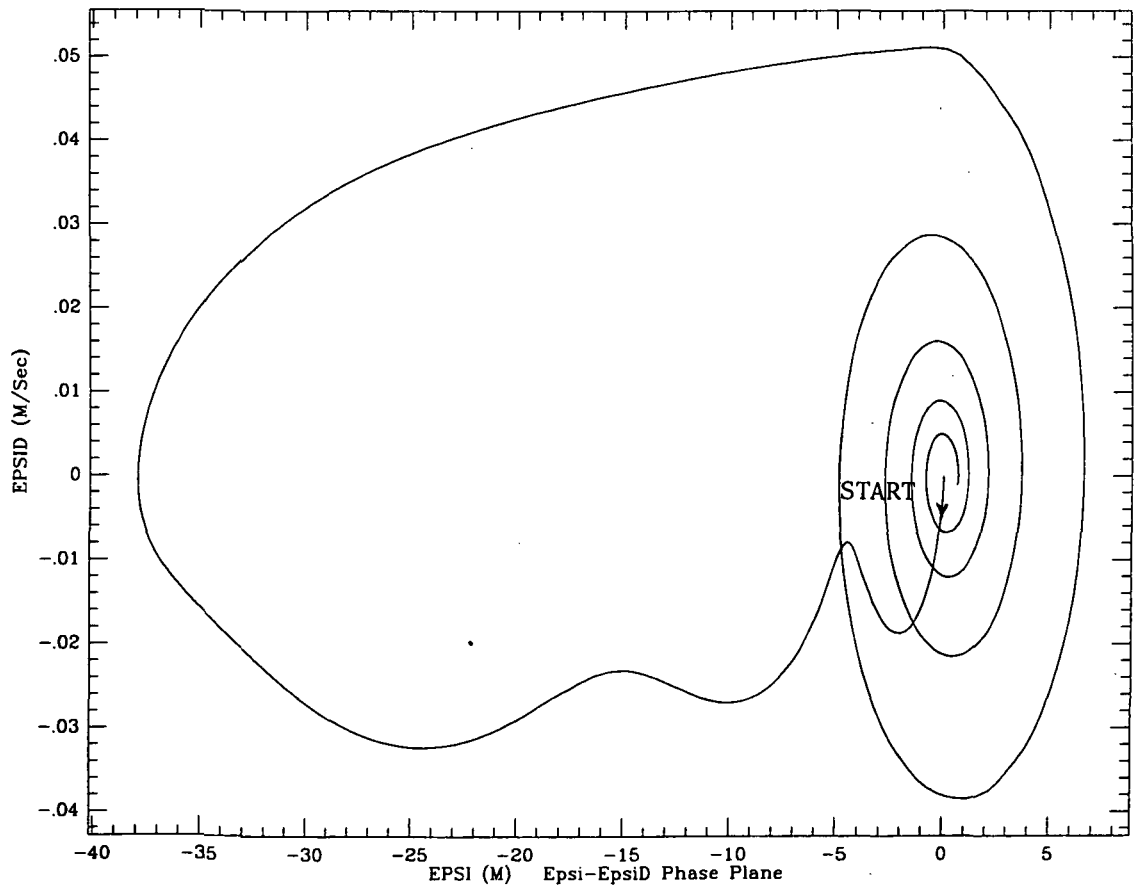

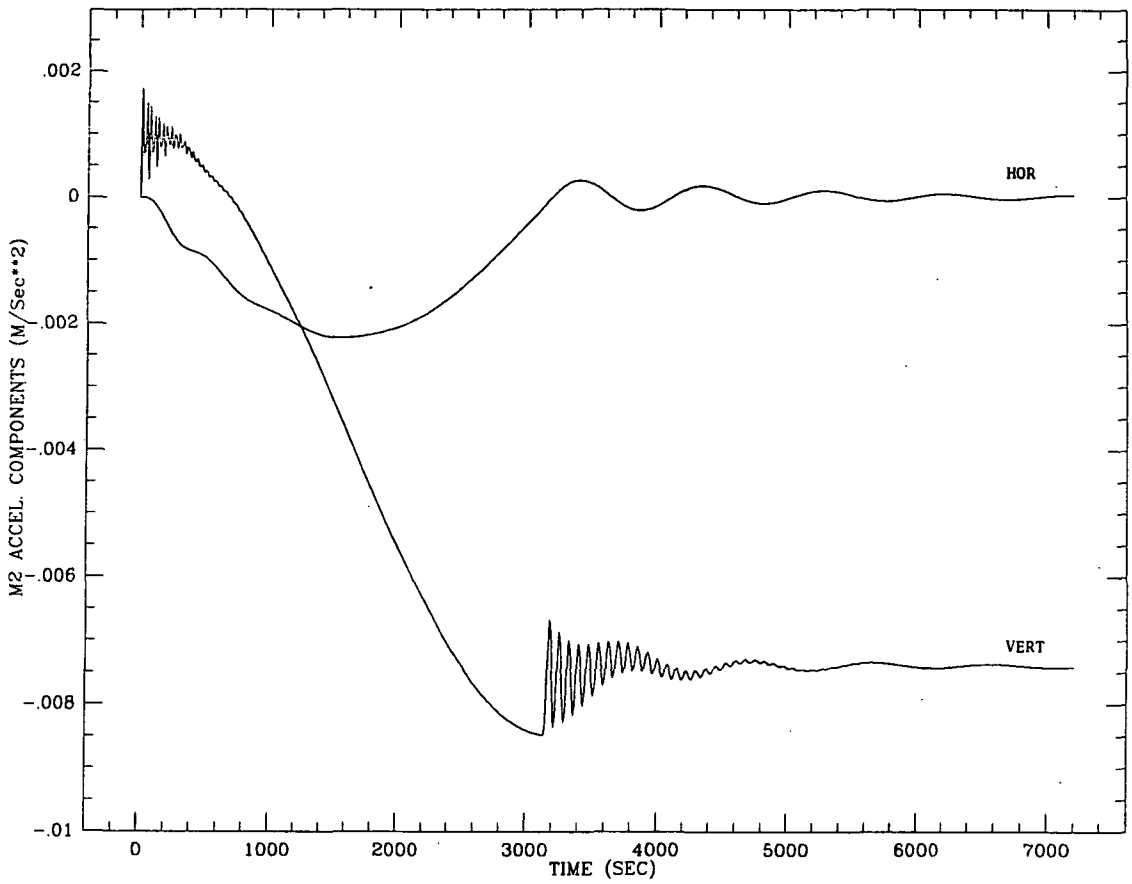

Figure 2.6.1g↑

Figure 2.6.1h↓

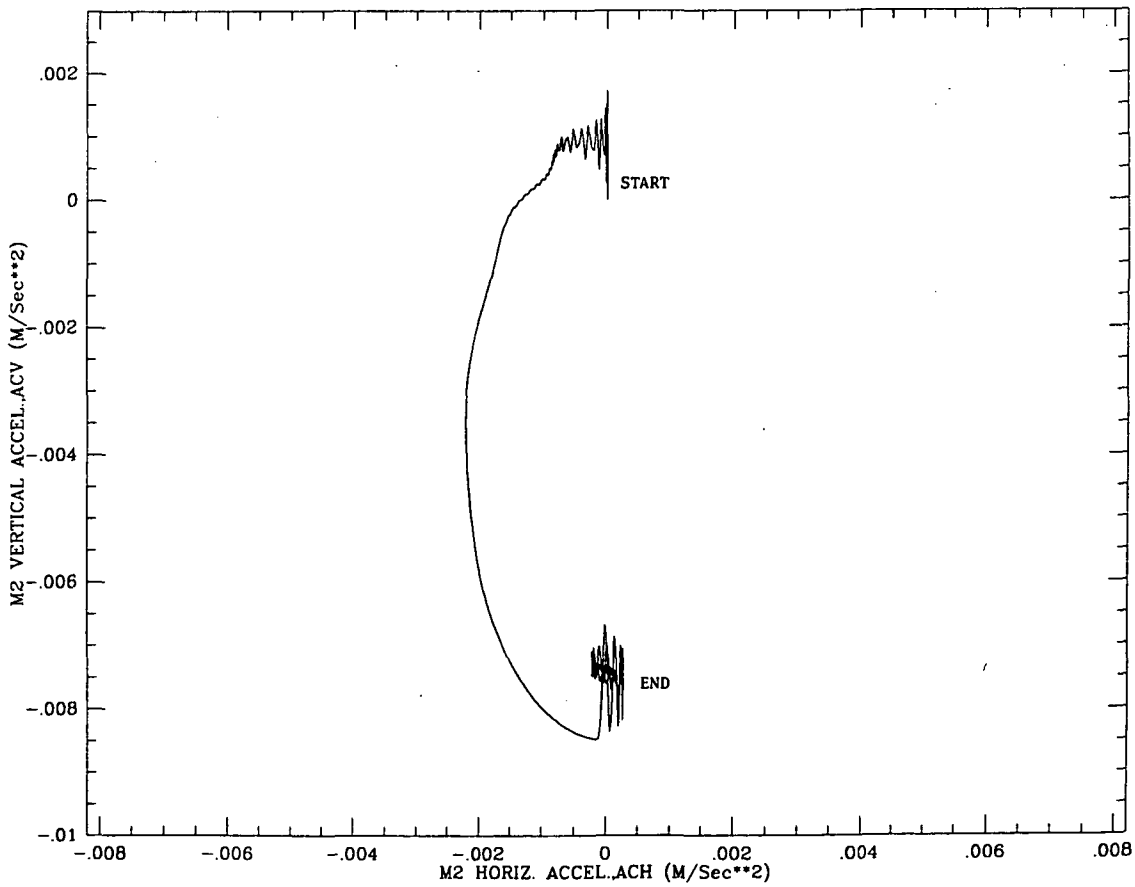

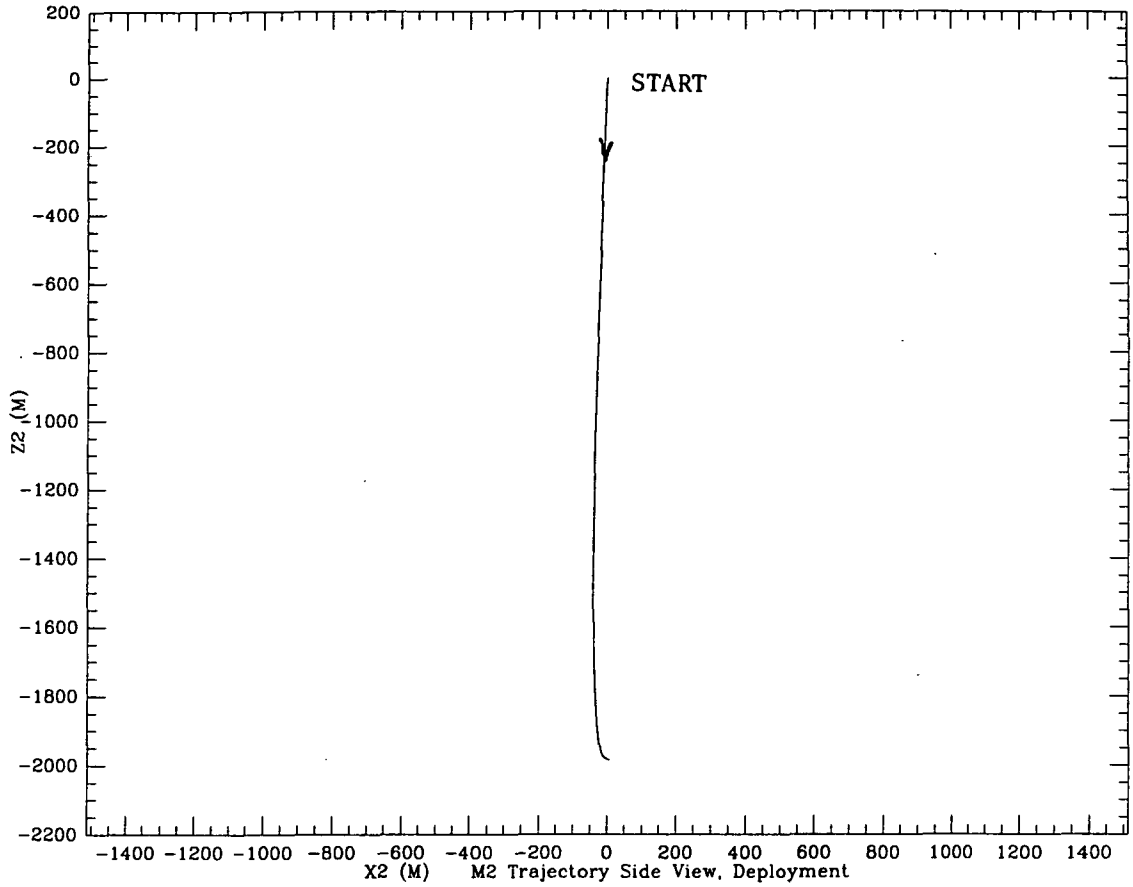

Figure 2.6.1i

Figure 2.6.1ℓ

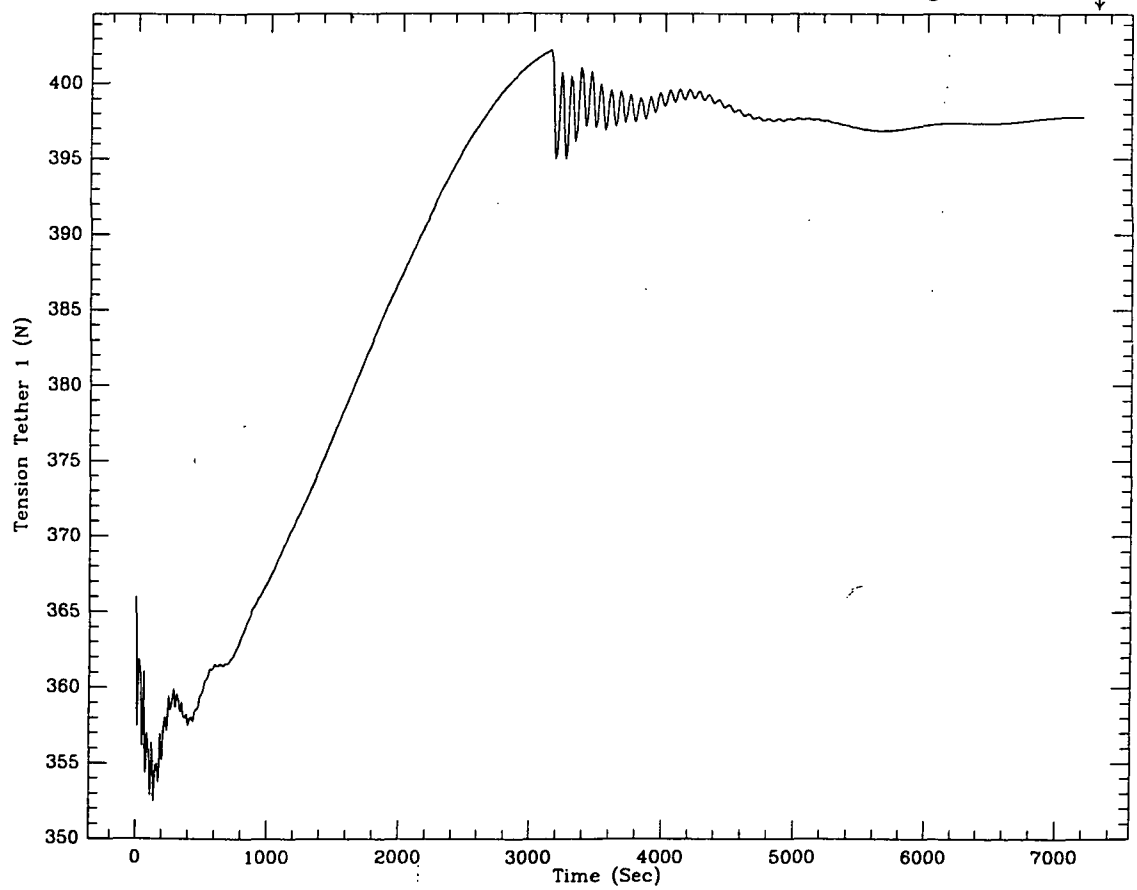

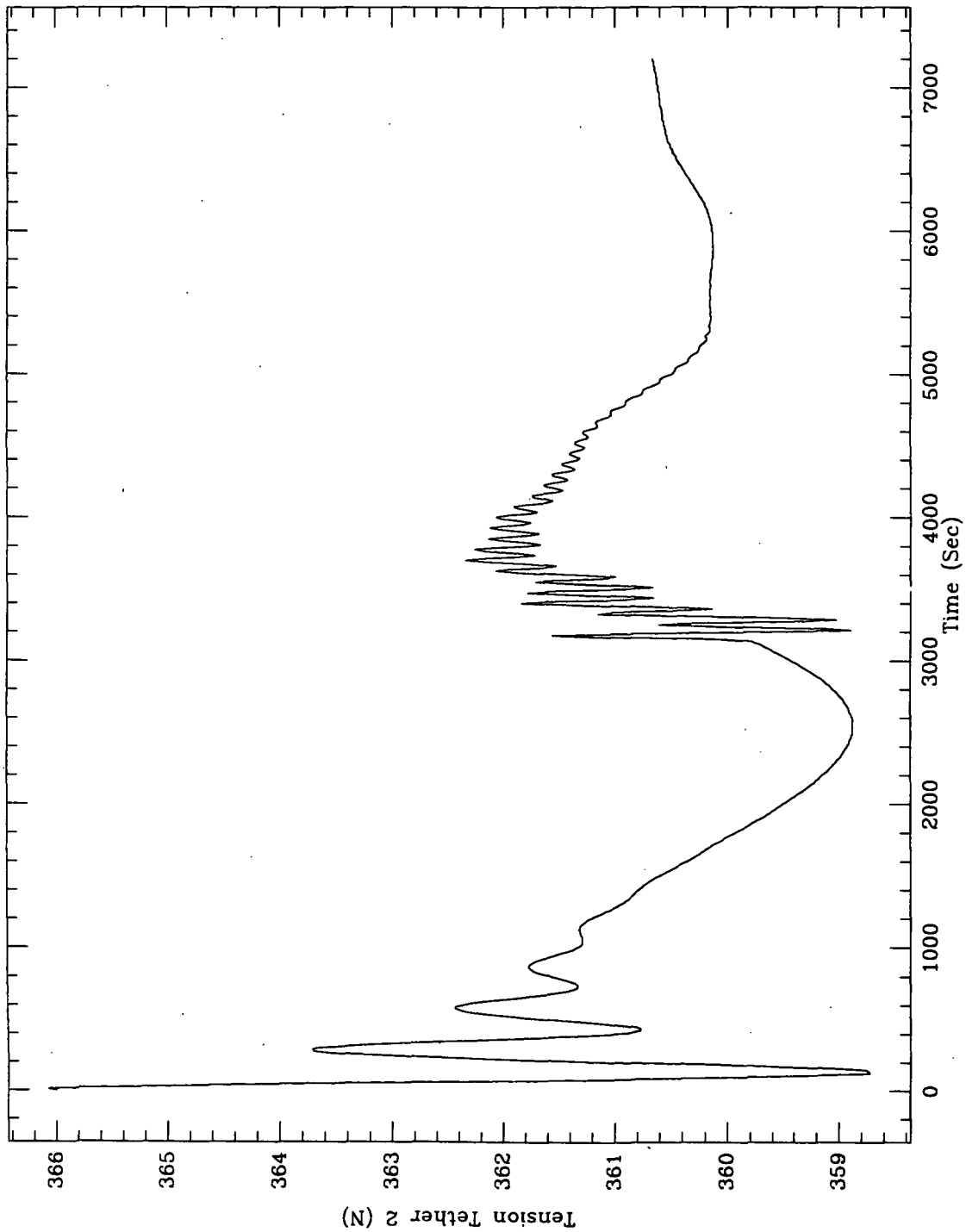
Tension Tether 2 (N)
366
365
364
363
362
361
360
359
0
1000
2000
3000
4000
5000
6000
7000
Time (Sec)

Figure 2.6.1m

The two constants α and β set the slope of the curve, β having been introduced in particular to slow down the acceleration phase (initial phase) of the control law. Results from a simulation with $2\Delta\ell_c$ = 2000 m, α = 1/2000 sec^{-1}, β = 1/1000 sec^{-1} are shown in Figure 2.6.2a-m. The sequence of plots is equivalent to the one previously illustrated. Note that the transient phase at the end of the maneuver has disappeared. In the same 7200 sec time frame the system reaches a quieter state than in the previous simulation. The initial transient phase is still there; it is partially due to the imperfect initial conditions. Figure 2.6.2g shows the acceleration components in the local orbiting reference frame at the middle platform. Note that at the end of the maneuver the horizontal acceleration component has completely disappeared while the vertical component has reached its steady state value.

2.7 Concluding Remarks

The newly developed Cartesian coordinate model provides a very convenient tool for analyzing multi-mass tethered systems. The new model of the 3-mass tethered constellation has been used to perform simulations which show the capabilities and the limitations of the tether system with respect to the reproduction of predetermined acceleration profiles on board the middle platform. Sinusoidal vertical acceleration variations of the desired frequency and amplitude can be obtained at the expense of a smaller horizontal acceleration component. This component deflects the total acceleration from the local vertical during the sinusoidal motion of the middle platform.

The "g-tuning" capability has been also demonstrated. An open loop control law that provides a satisfactory dynamic response has been devised. The middle

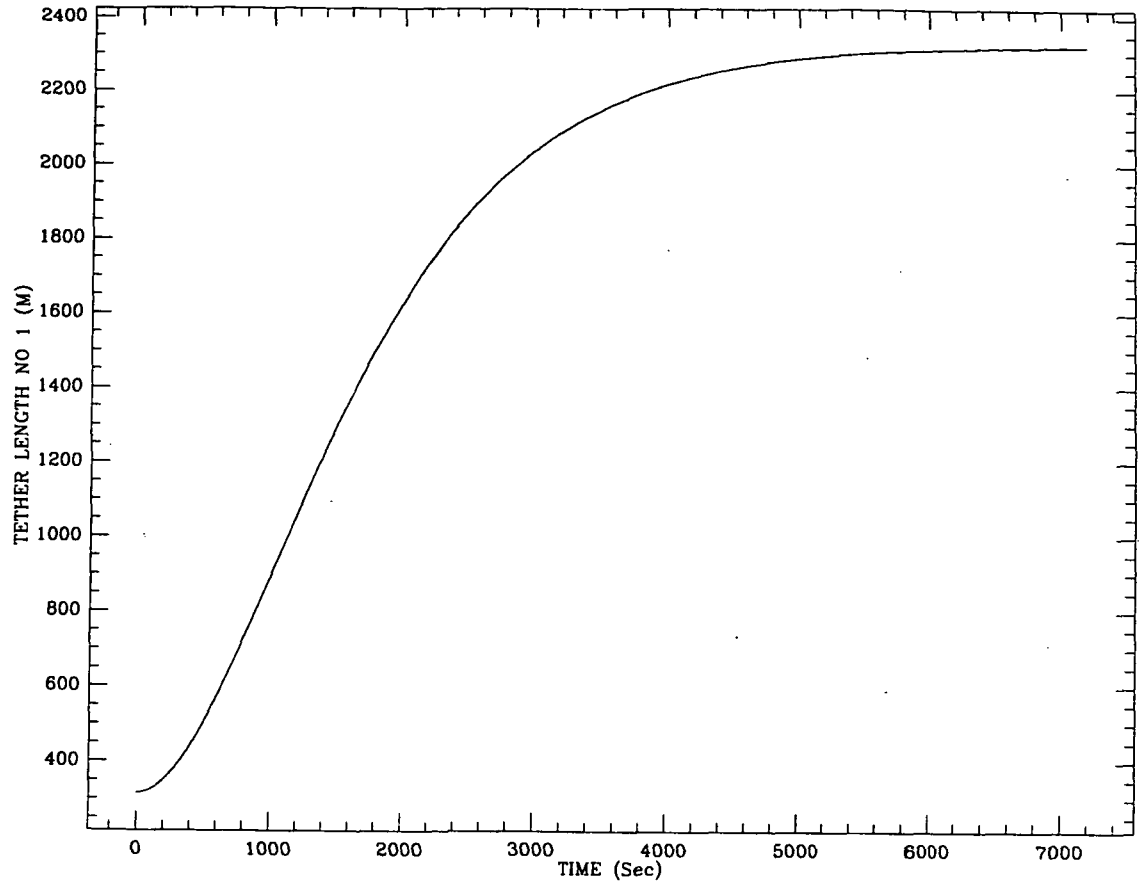

Figure 2.6.2a↑

Figure 2.6.2b↓

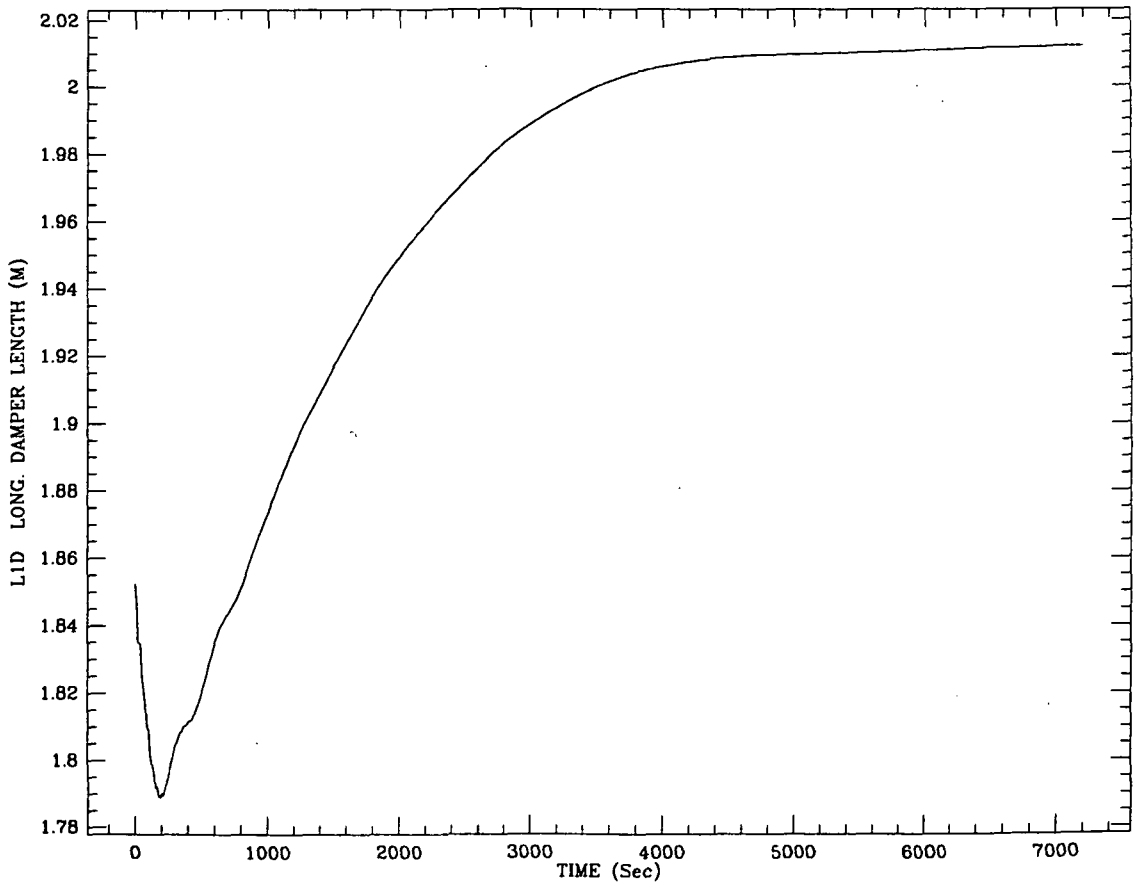

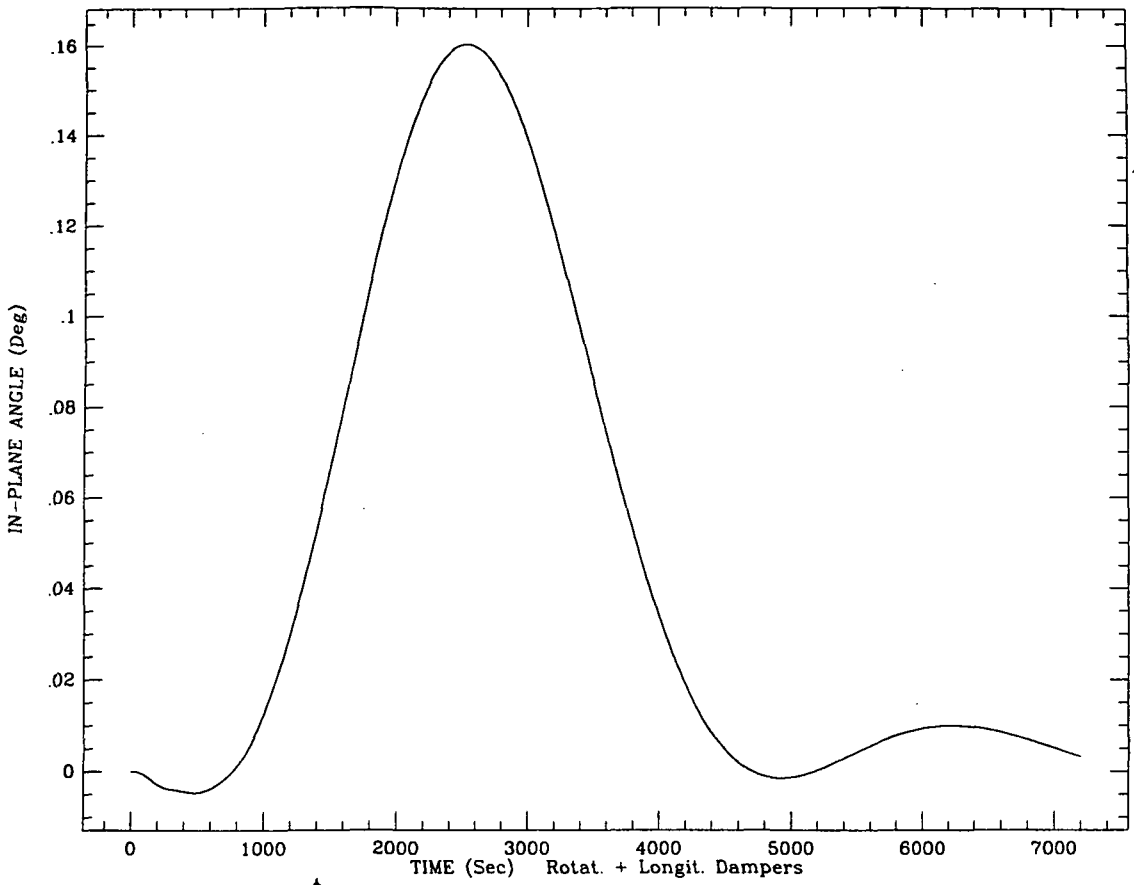

Figure 2.6.2c

Figure 2.6.2d

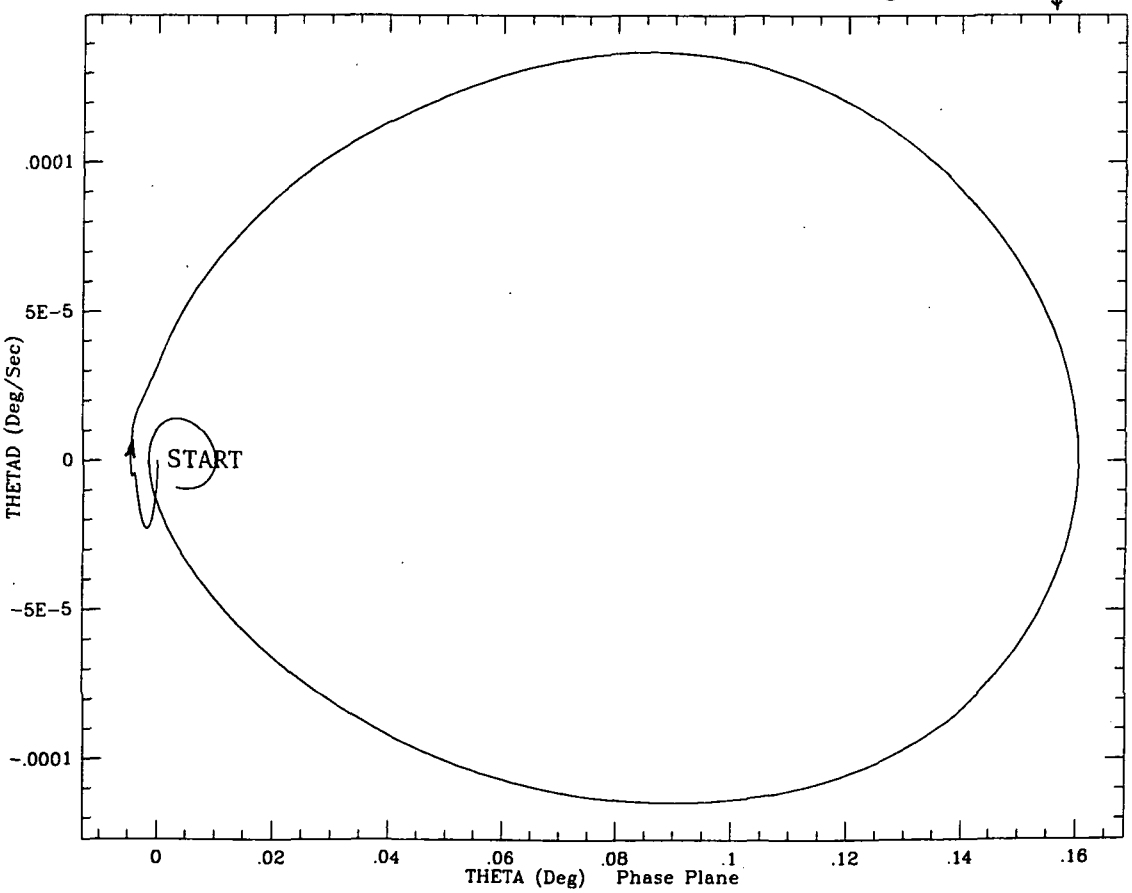

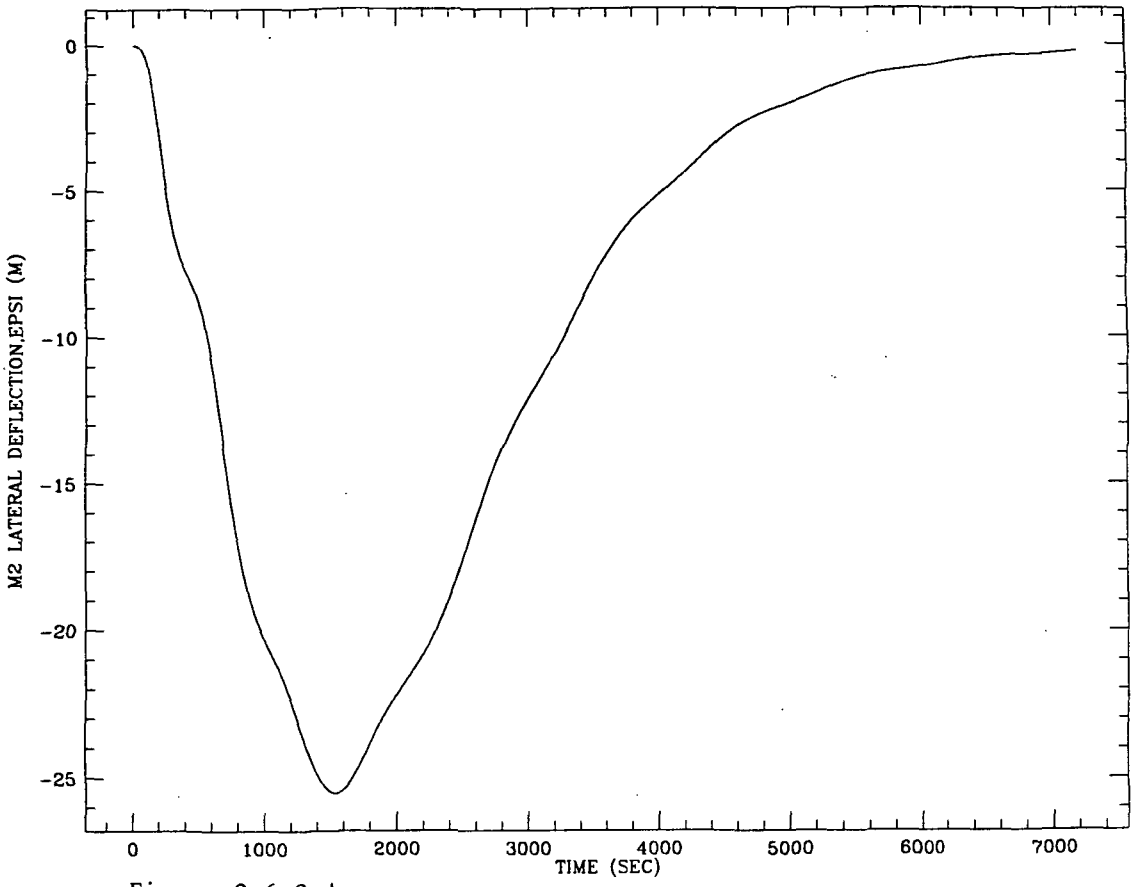

Figure 2.6.2e↑

Figure 2.6.2f↓

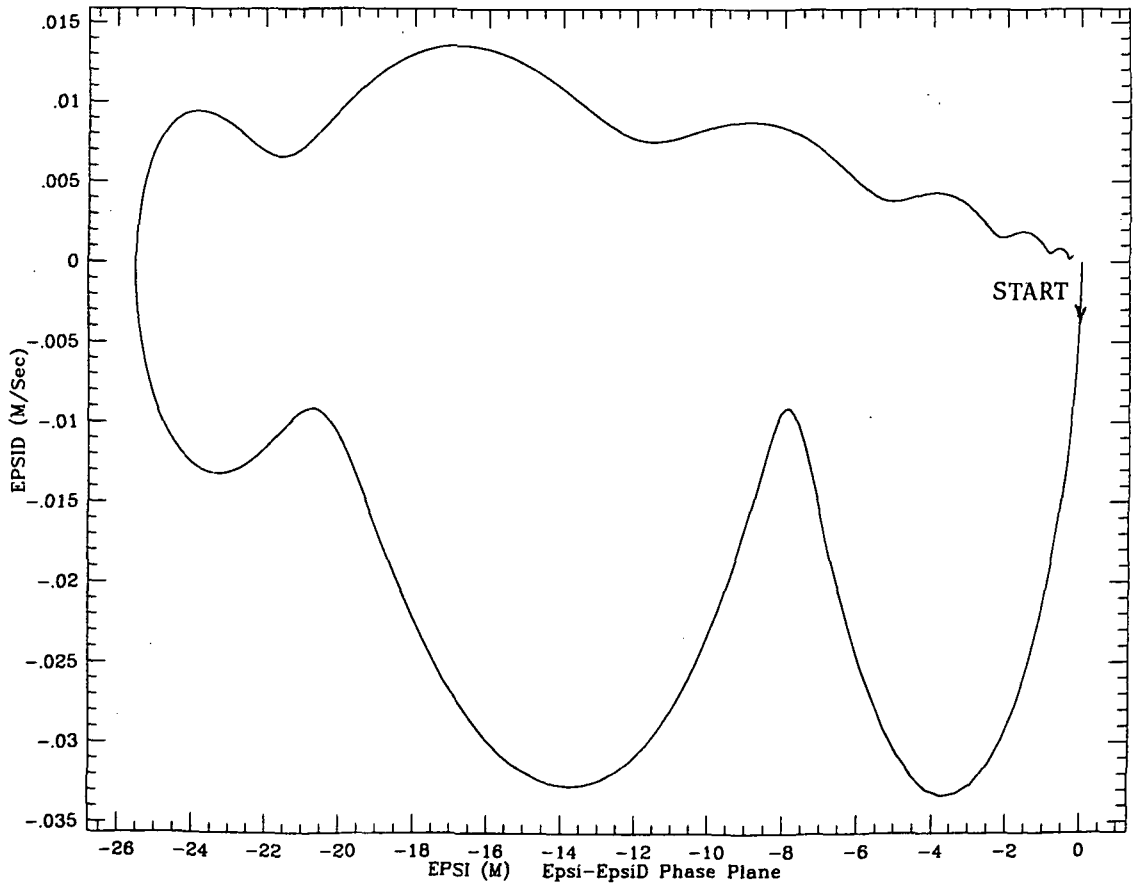

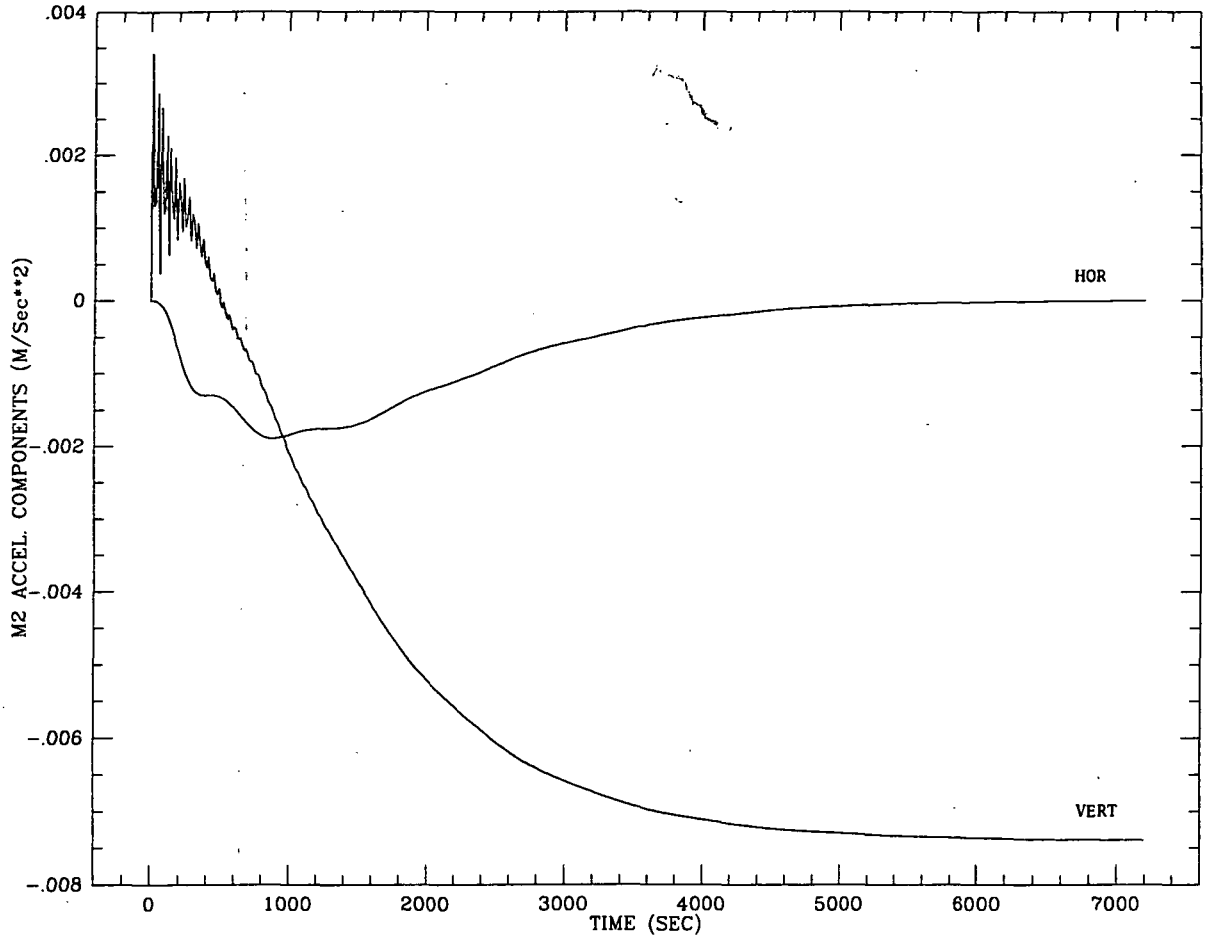

Figure 2.6.2g↑

Figure 2.6.2h↓

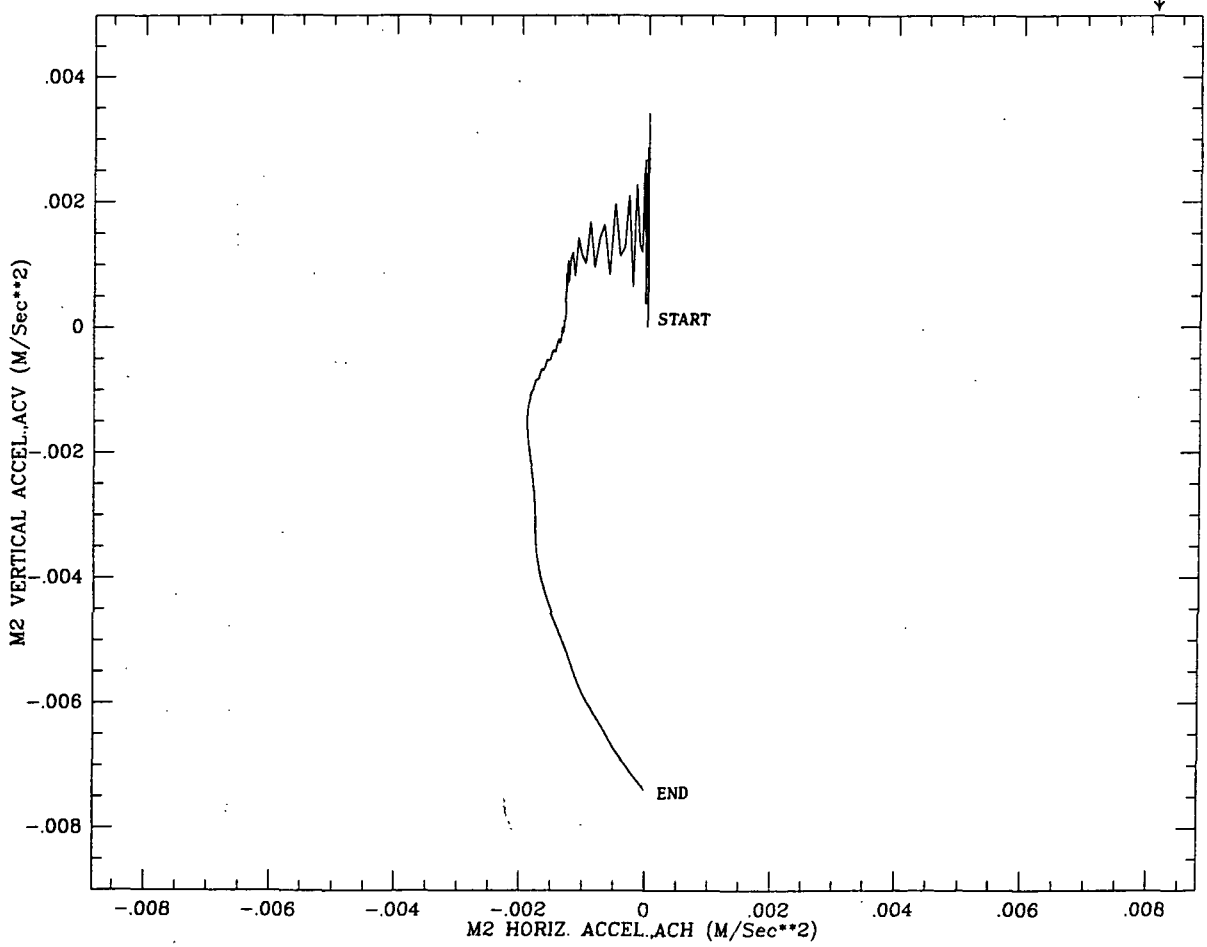

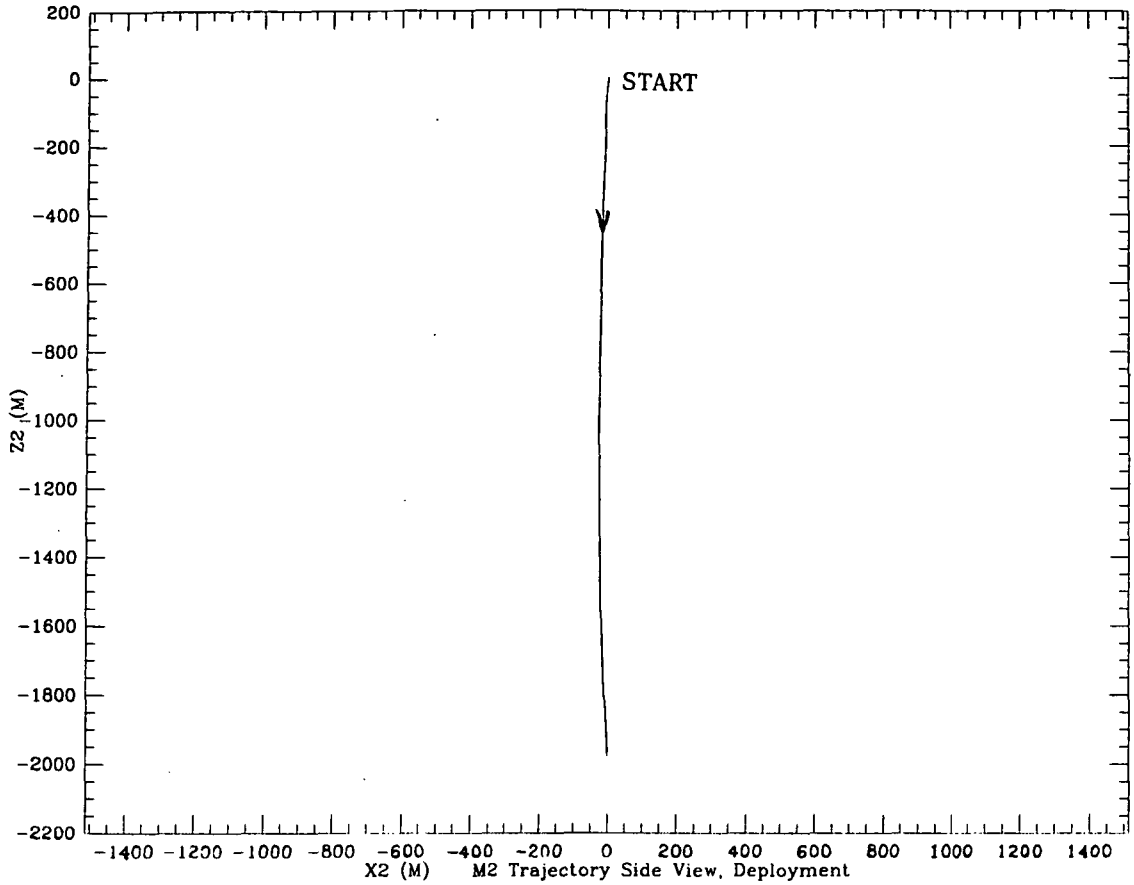

Figure 2.6.2i

Figure 2.6.2l

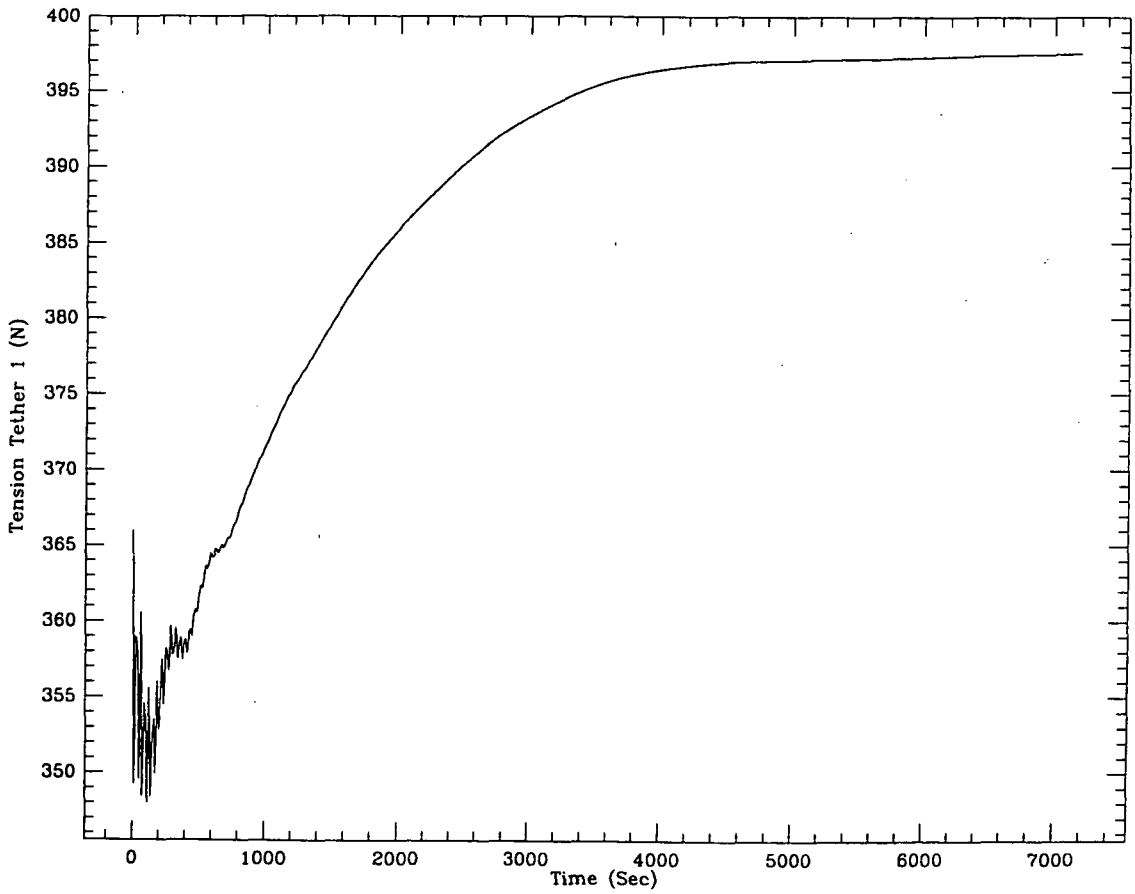

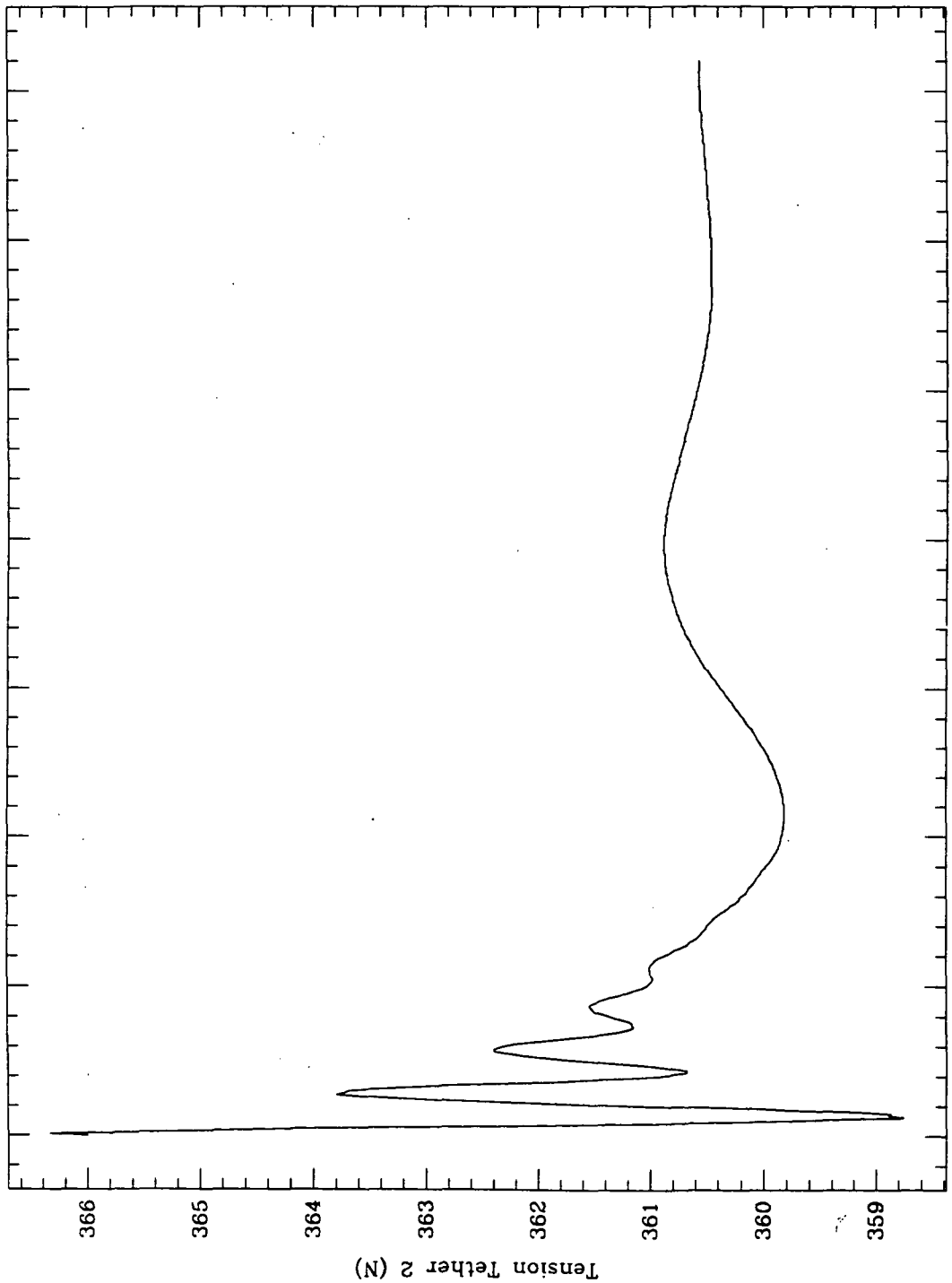
Tension Tether 2 (N)
366
365
364
363
362
361
360
359
0
1000
2000
3000
4000
5000
6000
7000
Time (Sec)

Figure 2.6.2m

mass is moved from the system C.M. to the desired location along the tether according to a modified hyperbolic tangent control law. Time constants for the control law have been derived in order to have a satisfactory transient response.

3.0 PROBLEMS ENCOUNTERED DURING THE REPORTING PERIOD

None

4.0 ACTIVITY PLANNED FOR THE NEXT REPORTING PERIOD

During the next reporting period further studies will be performed on the "g-tuning." We will investigate the case of displacing the middle mass from a position near the Space Station to the zero-g point in order to achieve a zero acceleration condition. We will also investigate the effect, upon the overall dynamics of the constellation, of a fast displacement of the middle mass from one tether tip to the other.